PHASE TRANSFORMATIONS AND SURFACE CHEMISTRY OF SECONDARY IRON MINERALS FORMED FROM ACID MINE DRAINAGE

by

Jörgen Jönsson

Akademisk avhandling

som med tillstånd av rektorsämbetet vid Umeå Universitet för erhållande av Filosofie Doktorsexamen framlägges till offentlig granskning vid Kemiska institutionen, sal KB3B1, KBC-huset, fredagen den 12 december 2003, kl 13.00.

Fakultetsopponent: Dr. Douglas B. Kent, U.S. Geological Survey, Menlo Park, USA.

ISBN 91-7305-552-2

Printed by Solfjädern Offset AB
Umeå, Sweden, 2003

TITLE PHASE TRANSFORMATIONS AND SURFACE CHEMISTRY OF SECONDARY IRON MINERALS FORMED FROM ACID MINE DRAINAGE

AUTHOR Jörgen Jönsson

ADDRESS Department of Chemistry, Inorganic Chemistry, Umeå University, SE-901 87 Umeå, Sweden

ABSTRACT

The mining of sulphidic ore to extract metals such as zinc and copper produces huge quantities of waste material. The weathering and oxidation of the waste produces what is commonly known as Acid Mine Drainage (AMD), a dilute sulphuric acid rich in Fe(II) and heavy metals. This thesis serves to summarise five papers reporting how the precipitation of Fe(III) phases can attenuate the contamination of heavy metals by adsorption processes.

Schwertmannite ($Fe_8O_8(OH)_6SO_4$) is a common Fe(III) mineral precipitating in AMD environments at pH 3-4. The stability and surface chemistry of this mineral was investigated. It was shown that the stability depended strongly on pH and temperature, an increase in either promoted transformation to goethite (α-FeOOH). Two pH dependent surface species of SO_4^{2-} were detected with infrared (ATR-FTIR) spectroscopy.

The adsorption of Cu(II), Pb(II) and Zn(II) to schwertmannite occurred at lower pH than to goethite, whereas Cd(II) adsorption occurred in a similar pH range on both schwertmannite and goethite. Extended x-ray absorption fine structure (EXAFS) spectroscopy suggests two surface species for Cu(II) and Cd(II) at the schwertmannite surface. Cu(II) adsorbs monodentately and Cd(II) bridging bidentately to adsorbed SO_4^{2-}. Both metal ions also adsorb in a bridging bidentate mode to the surface hydroxyl groups. At pH 7.5 up to 2.7 μmol Cd(II) m^{-2} could be adsorbed to schwertmannite, indicating a large adsorption capacity for this mineral.

The acid-base properties of two NOM samples were characterised and could be well described as diprotic acids below pH 6. The adsorption of NOM to schwertmannite and goethite was very similar and adsorption occured in a very wide pH range.

High concentrations of NOM increased the adsorption of Cu(II) to goethite at low pH whereas a slight decrease was noted at low concentrations of NOM. No effect was detected in the schwertmannite system.

The formation of Fe(III) phases from precipitation of AMD was shown to be very pH dependent. At pH 5.5 a mixture of minerals, including schwertmannite, formed whereas at pH 7 only lepidocrocite (γ-FeOOH) formed. The concentration of Zn(II) in AMD could by adsorption/coprecipitation be reduced to environmentally acceptable levels.

KEYWORDS schwertmannite, goethite, lepidocrocite, acid mine drainage, sulphate, natural organic matter, mineral surface, infrared spectroscopy, EXAFS, XRD, ternary surface complex, copper(II), cadmium(II), lead(II), zinc(II).

ISBN 91-7305-552-2 71 pages and 5 papers

PHASE TRANSFORMATIONS AND SURFACE CHEMISTRY OF SECONDARY IRON MINERALS FORMED FROM ACID MINE DRAINAGE

Jörgen Jönsson
Department of Chemistry, Inorganic Chemistry
Umeå University
SE-901 87 Umeå, Sweden

This thesis contains a summary and a discussion of the following papers, referred to in the text by their numbers 1-5.

1. Schwertmannite precipitated from acid mine drainage: Phase transformation, sulphate release and surface properties
   Jörgen Jönsson, Per Persson, Staffan Sjöberg and Lars Lövgren
   Submitted to *Applied Geochemistry*

2. Adsorption of Cu(II) and Cd(II) to schwertmannite precipitated from acid mine drainage - An EXAFS study
   Jörgen Jönsson, Julia Jönsson, John Wells, Lars Lövgren, Staffan Sjöberg, and Per Persson
   Manuscript

3. Adsorption of Cu(II) to schwertmannite and goethite in the presence of natural organic matter
   Jörgen Jönsson, Staffan Sjöberg, and Lars Lövgren
   Manuscript

4. Evaluation of different approaches to quantify strong organic acidity and acid-base buffering of organic-rich surface waters in Sweden
   Stephan Köhler, Jakub Hruška, Jörgen Jönsson, Lars Lövgren and Stephen Lofts
   Water Research, 2002, 36, 4487-4496

5. Precipitation of secondary Fe(III) minerals from acid mine drainage
   Jörgen Jönsson, Julia Jönsson and Lars Lövgren
   Manuscript

Papers of interest but not included in the thesis:

Sorption properties of secondary iron precipitates in oxidized mining waste
Jörgen Jönsson and Lars Lövgren
Proceedings from the 5th International Conference on Acid Rock Drainage, Denver, Colorado, USA, May 21-24, 2000, pp. 115-123.

Attenuation of metals by sorption to secondary iron precipitates
Jörgen Jönsson and Lars Lövgren
Proceedings from Securing the Future, International conference on Mining and the Environment, Skellefteå, Sweden, June 25-July 1, 2001, pp. 320-326.

CONTENTS

1 INTRODUCTION

Metals are very important in today's society; we use metals daily both at home and at work and it is hard to imagine what life would be like without them. The raw material for metal production comes from ore excavated in a mine. The mining activities inevitably produce waste material that can cause unwanted pollution in the areas around the mines. A very dramatic kind of pollution occurs when dams containing the waste material fail, such as the tailings dam at the Aznalcóllar/Los Frailes Ag-Cu-Pb-Zn mine in Spain in 1998. A far more common, and less dramatic type of pollution is that of Acid Mine Drainage (AMD), the drainage water from sulphidic mine waste and mines. AMD can be extremely acidic (pH<0) with very high concentrations of SO_4^{2-} (760 g dm^{-3}) and metals (200 g dm^{-3})[1]. Fortunately, most AMD is not this extreme but pH values between 3 and 4 are commonly encountered[2]. The problem with AMD arises because the ore that is excavated in a mine is not pure metal. On the contrary, most of the ore actually end up as waste. To extract the desired metal, the ore is finely ground in a mill and the mineral grains containing the metal are removed by a flotation process. The waste, a finely ground sand, is called tailings and are deposited in dams such as that in Aznalcóllar. In the tailings we find the source of AMD, which is mainly pyrite (FeS_2), ubiquitous in tailings from sulphidic ore. Oxidation and weathering of pyrite (Section 1.1) produces AMD, i.e. sulphuric acid and dissolved metal ions. The most common metal ion in AMD is Fe(II) which can be oxidised to Fe(III) and re-precipitate as ochre iron oxide coatings in streams affected by AMD (Section 1.2).

The problem with AMD is not new. Rio Tinto got the name from its red colour partly due to mining activities started centuries ago. The mining industry is fully aware of the problem and large financial and scientific resources have been devoted over the years in search of economically and technically feasible methods to decrease the impact of AMD. The solution to the problem is well known: prevent water, oxygen and bacteria from reaching the tailings. This, however, is often very costly. Among the methods used today are:

1. soil cover, where the tailings are covered with a soil of low hydraulic conductivity to reduce diffusion of O_2 and infiltration of H_2O[3].
2. water cover, the construction of an artificial lake to reduce O_2 diffusion[4].
3. reactive barriers, where AMD can be neutralised and metal ions precipitated[5].
4. (constructed) wetlands, to adsorb and precipitate metal ions[6].

5. liming, to neutralise AMD and precipitate metal hydroxides.

All of these methods have limitations and drawbacks, either economically or technically; soil covers are expensive, lakes can not be constructed everywhere, barriers and wetlands can be overwhelmed by Fe(III) precipitates and liming has to be maintained for a long time. As a complement to the above mentioned methods, the process of natural attenuation is frequently discussed. The essence of this concept is to utilise processes or substances that will inevitably take place, be formed or are present and to optimise their use to the full potential. In order to reduce the metal ion concentration in AMD, natural attenuation by particles can be seen as a sequence of steps:

1. formation of particles
2. association of metal ions with the particles by adsorption or co-precipitation
3. aggregation and sedimentation of particles
4. transformation and stabilisation of precipitates

It is in this context, and especially in steps 1, 2 and 4 of the above sequence, that this thesis is intended to contribute.

The rest of the introduction will glance briefly at subjects that not all readers may be familiar with such as pyrite oxidation (Section 1.1), secondary precipitates (1.2), surface complexation (1.3) and Natural Organic Matter (1.4). The introduction ends with the objective of this thesis (Section 1.5).

1.1 Pyrite weathering and oxidation

As mentioned above, oxidation and weathering of pyrite is the source of AMD. The oxidation of pyrite is often described by the single equation given in Equation (1.1):

$$FeS_2(s) + 3.75\ O_2(g) + 3.5\ H_2O(l) \rightleftarrows Fe(OH)_3(s) + 4\ H^+(aq) + 2\ SO_4^{2-}(aq) \qquad (1.1)$$

As can be seen, the reaction is dependent on oxygen and water but the oxidation rate is also dependent on temperature, pH and the presence of Fe- and S-oxidising bacteria. This reaction is a simplification as the oxidation of pyrite and precipitation of Fe is usually separated in both time and place. First of all, the oxidation of S_2^{2-} and Fe^{2+} does not normally occur simultaneously as S_2^{2-} is more easily oxidised than Fe^{2+}[7]:

$$0.5\ S_2^{2-} + 4\ H_2O \rightleftarrows SO_4^{2-} + 7\ e^- + 8\ H^+ \qquad E^0 = 0.24\ V \qquad (1.2)$$

$$Fe^{2+} \rightleftarrows Fe^{3+} + e^- \qquad E^0 = 0.77\ V \qquad (1.3)$$

Thus, S_2^{2-} is first oxidised by either O_2 or Fe^{3+} according to Equation (1.4) and (1.5), respectively:

$$FeS_2(s) + 3.5\ O_2(g) + H_2O(l) \rightleftarrows Fe^{2+}(aq) + 2\ SO_4^{2-}(aq) + 2\ H^+(aq) \quad (1.4)$$

$$FeS_2(s) + 14\ Fe^{3+}(aq) + 8\ H_2O(l) \rightleftarrows 15\ Fe^{2+}(aq) + 2\ SO_4^{2-}(aq) + 16\ H^+(aq) \quad (1.5)$$

This oxidation can either be abiotic or catalysed by S-oxidising bacteria such as *Acidithiobacillus ferrooxidans*. For a recent review regarding the importance of bacteria in pyrite weathering, see Ebenå[8]. That S_2^{2-} is more easily oxidised than Fe^{2+} can be seen in many AMD waters, as the concentrations of Fe^{2+}, SO_4^{2-} and H^+ are high, see e.g. Paper 5 where the formation of Fe(III) precipitates from AMD is studied. Fe^{2+} is then oxidised according to Equation (1.6):

$$Fe^{2+} + 0.25\ O_2 + H^+ \rightleftarrows Fe^{3+} + 0.5\ H_2O \quad (1.6)$$

This oxidation can also be abiotic or catalysed by Fe-oxidising bacteria, e.g. *A. ferrooxidans*. The importance of Fe-oxidising bacteria in pyrite oxidation can be understood from examining Equation (1.5). Here, Fe^{3+} oxidises pyrite rapidly and is reduced to Fe^{2+}. Bacteria then oxidise Fe^{2+} back to Fe^{3+} (Equation 1.6) and more pyrite can be oxidised. As the pyrite is weathered and dissolved, the trace elements that are present will also be dissolved[2]. It should be noted that monosulphides such as pyrrhotite ($Fe_{1-x}S$) are more easily oxidised than pyrite[9] but are usually present in lower concentrations than pyrite.

1.2 Secondary precipitates

The high concentrations of dissolved Fe(II) and SO_4^{2-} in AMD may also accompanied by relatively high concentrations of e.g. Al(III) and Mn(II). As the AMD reaches surface waters and is neutralised the metal ions will precipitate, forming secondary precipitates of varying mineralogy. The three metal ions mentioned precipitate in a very specific order. Fe(III) precipitates at the lowest pH, below 4, followed by Al(III) around pH 5 whereas Mn(II) does not precipitate until about pH 8[10-12]. The order can be visible in streams where ochre Fe(III) precipitates form up-stream of whitish Al(III) precipitates. The pH values at which the metals precipitate may however change slightly, depending on factors such as temperature and concentration as more soluble precipitates can form due to evaporation.

The precipitation of $Fe(OH)_3$ as described in Equation (1.1) is a simplification as different solid Fe(III) phases form at different pH and SO_4^{2-} concentrations. At pH below 3, different forms of jarosite,

$(H,K,Na)Fe_3(OH)_6(SO_4)_2$, precipitate. In waters having pH values in the range of 2.8 to 4.5, schwertmannite ($Fe_8O_8(OH)_6SO_4$) dominates. From pH 4.5 to 6.5, a mixture of schwertmannite and ferrihydrite ($Fe_2O_3 \cdot 1.8\ H_2O$) precipitates, whereas at higher pH only ferrihydrite or a mixture of ferrihydrite and goethite (α-FeOOH) precipitates[13,14]. Mixtures of the different minerals are often observed, partly due to transformation processes to thermodynamically more stable minerals. Soluble Fe(II) and mixed Fe(II) and Fe(III) phases can also be formed, storing acidity that can have a severe ecological impact in the event of rainfall. The solid phases formed are seldom pure and often contain impurities of trace element due to coprecipitation. Besides coprecipitation, the mineral phases can remove dissolved trace elements from solution by adsorption, thus making the field of sorption processes interesting in terms of natural attenuation of metal ions. The potential for removal is possibly large as the phases formed often have a large surface area and the concentration of Fe(II) and Fe(III) in AMD far exceeds that of the trace elements[2].

1.3 Sorption processes

At the oxide-water interface a number of reactions can take place, e.g. acid-base reactions, ion exchange and formation of complexes with solutes. The reactions take place at specific sites at the surface, the surface sites. The reactivity of the surface sites arises from coordinative unsaturation of the oxide surface which leads to formation of surface hydroxyl groups. It is these hydroxyl groups that form the surface sites[15]. The hydroxyl groups coordinate with different number of bonds to the metal ions in the oxide and the reactivity of the hydroxyl groups are affected by the number of bonds and the charge of the metal ion in the oxide. Generally speaking, singly coordinated hydroxyls are the most reactive followed by triply coordinated groups. Doubly coordinated groups are relatively unreactive in the pH range encountered in most natural waters[16].

Cations and anions can form complexes at the surface sites in a way similar to the formation of complexes in solution. There are however some important differences. Firstly, the adsorbing ion can form two different types of complex. With a direct bond (largely covalent in character) with the surface, an inner sphere complex is formed. Weaker outer sphere complexes are formed when the bond is mainly due to electrostatic attractions or hydrogen bonding. The surface and the adsorbing ion are then separated by at least one water molecule. Strictly speaking, these two types of complexes are not unique for surfaces as they exist in solution as well. Secondly, the formation of surface complexes and the (de)protonation of the surface cause

a charge to develop at the oxide-water interface. The charged surface attracts oppositely charged ions from the solution and an electrostatic double layer is developed. The charging and electrostatic double layer affects the sorption processes. This effect can be handled by incorporating an electrostatic double layer model into a surface complexation model[17].

1.4 Natural Organic Matter

Sooner or later AMD finds its way out from the source, the deposit, and encounter the surrounding recipient where AMD can be neutralised and secondary precipitates formed as described above. The area receiving AMD probably comprises surface water and, hopefully, vegetation. As vegetation eventually dies and decomposes, the carbon from the vegetation is released into the surface water and encounters the components of AMD. Here a very complex system is formed as, more or less simultaneously, different chemical reactions can take place; precipitation, coprecipitation, acid-base reactions, and complex formation both at the solid-water interface and in solution. To understand all of the processes, it is of benefit to investigate the different sub-systems separately, whereafter the different model systems can be linked together. Of the components in this mixture, the various organic compounds formed are the most complex and diverse and deserve special attention regarding acid-base, sorption and complexing properties.

The organic molecules in natural waters are very heterogeneous in both size and composition and are often referred to as Natural Organic Matter, abbreviated NOM. Another term closely related to NOM is Dissolved Organic Carbon (DOC), defined as the organic carbon passing through a filter, usually with a pore size of 0.45 μm. When discussing NOM, two groups of compounds are frequently mentioned; Fulvic Acids (FA) and Humic Acids (HA). Both are of high molecular weight with FA being the smaller in size though usually more abundant. HA is defined as the organic material precipitating at pH<2, where FA still is soluble. The amount of aqueous NOM varies between aquatic systems and so do the amounts of FA and HA. The highest concentrations of NOM are often found in bogs where up to 90% of the DOC pool may be made up of FA and HA. It is also in these waters the largest fraction of HA is observed, up to 35% of DOC[18].

NOM is proposed to be formed through different, interacting, pathways, e.g. microbial degradation of plant components, leaching from soil, polymerisation and ultraviolet oxidation. The pathways and starting material will differ from area to area, i.e. NOM in a lake in a cultivated area will not be the same as in a forest bog. Also, NOM is constantly changing due to microbial degradation and chemical alteration. However, even though NOM

might be different in different areas, the chemical properties are remarkably similar[19,20] (Paper 4). Hypothetical structures of humic matter have been proposed and these structures contain a rather large fraction of functional groups containing oxygen, e.g. carboxylic (-COOH) and phenolic (Ar-OH) groups. These groups can explain the acid-base buffering at different pH as well as the ability of NOM to complex with metal ions and mineral surfaces.

1.5 Objectives

In 1998 the MiMi (Mitigation of the Environmental Impact from Mining Waste) programme started with the overall goal to "devise methods for the safe disposal of mining waste and for the reliable prediction of their function over very long periods of time"[21]. MiMi is a joint effort between six universities, two firms of consultants and the mining companies Boliden and LKAB. The programme is funded by the Swedish Foundation for Strategic Environmental Research (MISTRA). The field site common for the project is the Kristineberg mine in northern Sweden. The present thesis is part of the MiMi subproject *Far Field Natural Attenuation* with the objective to "develop methods for an optimised utilisation of natural attenuation processes in structures for the passive treatment of drainage water"[21].

The objectives of this thesis have been to study the character and stability of secondary iron minerals precipitated from AMD as well as the sorption of metal ions to two of these minerals (schwertmannite and goethite) and the influence of NOM on the metal sorption.

2 TECHNIQUES AND EXPERIMENTAL PROCEDURES

The choice of an experimental technique depends on the information the experimentalist wishes to acquire and sometimes complementary techniques have to be used in order to answer certain questions. Macroscopic techniques (e.g. titrations and batch sorption experiments) can be employed to quantify processes in the system studied whereas microscopic techniques (often spectroscopic methods) answer questions regarding chemical processes on a molecular level. It could be argued that it is only important to be able to quantify e.g. how much of the metal ion will be adsorbed at a certain pH, but in order to make accurate models and predictions, information from combined macroscopic and molecular level techniques is necessary. In this work, a variety of techniques have been used in order to gather information concerning schwertmannite, goethite, NOM, and their sorption properties.

2.1 Materials

2.1.1 Schwertmannite

The schwertmannite sample used was collected at the Kristineberg Cu-Zn mine in 1998. To remove as many dissolved ions from the pore water and adsorbed metals from the surface as possible, the sample was repeatedly washed with 1 mM HNO_3 as described in Paper 1. The washed solid was dried at 40°C, ground and stored dry. The drying and grinding steps were performed to obtain a homogenous sample, as the sample was noticeably layered in the centrifuge tubes used in the washing procedure indicating size fractionation.

2.1.2 Goethite

Goethite was prepared by mixing solutions of $Fe(NO_3)_3$ and KOH according to Atkinson *et al.*[22]. The precipitate was allowed to age for at least six months to minimise changes in surface properties within the experimental period. During the ageing period the precipitate was washed several times to remove counter ions and excess base from solution and particle surfaces. The specific surface area was determined by the BET-method[23] to be 32.5, 39.9 and 42.1 $m^2\ g^{-1}$ for the three batches of goethite used.

2.1.3 NOM

NOM was sampled in January 1998 and April 1999 in a bog in Svartbergets Forest Research Area in northern Sweden (65°15’ N, 10°46’ E). The

concentration of NOM was increased by separation of ice by slow freezing at -20°C. The freezing out procedure was started within six hours after sampling and stopped when the remaining liquid volume was ~10% of the original sample volume. The concentrate was stored in a polyethylene bottle in a refrigerator to minimise possible bacterial activity and UV-degradation. Before use, the concentrate was filtered through an acid washed (10% HNO_3) 0.45 µm HA Millipore® filter.

2.1.4 Ionic media and pH

Dried $NaNO_3$ or NaCl was used to provide constant ionic strength (*I*). The use of a constant ionic strength is advisable when determining equilibrium constants as this keeps the activity coefficient (γ) for the different ions constant. Concentrations, rather than activities, can then be used in equilibrium calculations. This also has implications in reporting pH. When a study in this thesis was conducted in a constant ionic medium, the ionic medium in question was used as the outer filling solution in a combination electrode and the electrode was calibrated against an acid of known concentration in the same ionic medium and thus $pH = -\log[H^+]$. When a self-medium has been used, as is the case for some of the schwertmannite studies in Paper 1 and the precipitation study in Paper 5, the outer filling solution was a standard filling solution and the combination electrode was calibrated against commercial buffers and $pH = -\log\{H^+\}$.

2.2 Methods

2.2.1 Batch sorption experiments

This experimental technique is very useful for quantifying the amount of a substance that is adsorbed to or desorbed from a surface. The principle is quite simple; add the substance of interest to a mineral suspension, stir, wait and analyse the amount of the substance left in solution. The amount of the substance that has disappeared from solution has either been adsorbed or precipitated.

The scope of the adsorption experiments was to determine the amount of metals (Cd(II), Cu(II), Pb(II) or Zn(II)) and/or NOM adsorbed to the surface of schwertmannite or goethite as a function of pH and adsorbate/adsorbent ratios (Papers 2 and 3 and Chapter 5 and 6). In the experiments the mineral suspension was first transferred to a titration vessel. For goethite suspensions, the concentration of proton active hydroxyl groups at the surface was determined in the pH-range 2.6-2.9 by titrations[24]. Limitations of this procedure are discussed by Lützenkirchen et al.[25]. Metal solution

and/or NOM solution was then added. Acid or base were used to change pH, samples were collected at the desired pH values, transferred to test tubes and placed on an end-over-end turner. After 48 h the pH was measured and the test tubes centrifuged. The acidified supernatants were analysed for aqueous metal and/or NOM concentration. The metal concentration was analysed with AAS (flame atomic absorption spectroscopy) and NOM concentration was analysed with either a combustion method or UV spectroscopy.

The ionic strength dependence on the release of SO_4^{2-} from schwertmannite was studied at pH 3 in NaCl medium. The solid was added to the ionic medium and pH was adjusted, if necessary, with dilute HNO_3. After 3 h the pH was measured again, the samples were centrifuged and the supernatant was analysed for aqueous S content.

2.2.2 Potentiometric titrations

Many of the chemical reactions taking place in aqueous solutions and suspensions are pH dependent, e.g. formation of metal-ligand complexes, acid-base reactions of inorganic and organic acids, and the adsorption of ions to surfaces. It is therefore important to study the pH dependency of such reactions. Potentiometric titrations are very useful for studying these kinds of reactions as the method enables quantification of the change in $[H^+]$. A titration is usually carried out by addition of acid or base and $[H^+]$ is measured at equilibrium. With knowledge of volumes and concentrations, stoichiometry and thereby equilibrium constants can be calculated. This experimental technique was used to study the acid/base properties of NOM in Paper 3 and 4.

The potentiometric titrations were performed with a system for high-precision EMF titrations based on the setup described by Ginstrup[26] and illustrated in Figure 2.1. The key components for measuring the free $[H^+]$ are the Ag/AgCl reference electrode[27] in a "Wilhelm" type bridge[28] and the glass electrode. The two electrodes are connected to a voltmeter and the measured EMF value is registered by a computer. The additions of acid and base were made with a burette. For titrations with mineral suspensions, a stirring propeller was used to keep the suspension homogenous. This was preferred to a magnetic stirrer to avoid grinding of the mineral.

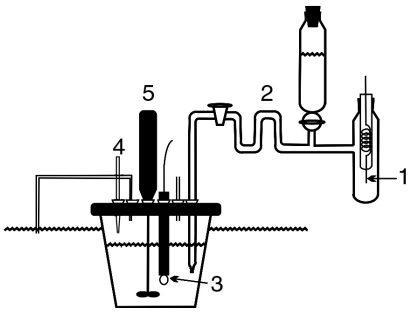

Figure 2.1 Setup used for potentiometric titrations. 1) reference electrode, 2) "Wilhelm" bridge, 3) glass electrode, 4) burette, 5) propeller. The titration vessel is partly immersed in an oil bath kept at 25.00°C.

Using the setup described above it is possible to determine the $[H^+]$ by measuring the EMF of the cell:

-Ag,AgCl | 0.01M NaCl+0.09M $NaNO_3$ || 0.1M $NaNO_3$ || eq. sol. | glass electrode+ (A)

or

- Ag,AgCl | X M NaCl || equilibrium solution | glass electrode + (B)

Most of the measurements have been performed in 0.100 M Na(NO_3) and then cell arrangement (A) has to be used. Some titrations have been carried out using Na(Cl) as background electrolyte and then cell arrangement (B) has been used with X = 0.020 or 0.600. The EMF (or *E*, in mV) of the cell is given by:

$$E = E_0 + g \log[H^+] + E_j \quad (2.1)$$

where E_0 is an apparatus constant, g = 59.16 mV at 25°C and the liquid junction potential E_j is calculated according to Sjöberg *et al*.[29]. E_j arises due to differences in concentrations over a liquid junction. Ions will diffuse over the liquid junction to eliminate the difference and this causes E_j to develop[30].Titration data were evaluated using the computer program LAKE[31].

2.2.3 pH-stat

The pH-stat technique may be described as a combination of batch sorption experiments and potentiometric titrations. The method can be used to determine adsorption isotherms, e.g. the maximum amount of a substance that can be adsorbed at a certain pH value although the risk of precipitation

of the added substance also has to be considered. This technique was employed in a number of studies as listed below.

The transformation of schwertmannite to goethite (Paper 1) was studied at pH 6 and 9 and divided into two experimental parts, one lasting a period of 6 h – 2 weeks and the other a period of 5-17 months. For the shorter time period an automatic pH-stat system was used. For the longer time period (5-17 months), pH was repeatedly adjusted manually to pH 6 or 9 with a strong base for the duration of the study. The automatic pH-stat system was also used to study the release of SO_4^{2-} from schwertmannite as a function of pH (Paper 1), the influence of SO_4^{2-} on NOM adsorption to goethite (Section 6.2), to acquire adsorption isotherms of NOM to goethite (Section 6.1) and to study which secondary iron minerals form from AMD (Paper 5). The metal adsorption capacity of the schwertmannite surface was studied at pH 7.5 with Cd(II) as a probe ion (Section 5.3). pH was adjusted manually in this study as the automatic pH-stat system was not able to handle the low buffering capacity in this system, resulting in too high pH values where the risk of $Cd(OH)_2$ precipitation was imminent.

2.2.4 Zeta potential

When studying sorption processes, the charge of the surface is very important as has been discussed in Section 1.3. Unfortunately it is not possible to measure the charge at the surface but what can be measured, or calculated rather, is the so-called zeta (ζ) potential. At the particle-water interface, the first few layers of water molecules are stagnant and move along with the particle. The boundary between the water molecules moving with the particle and the bulk of water is called the slip plane. It is the potential at the slip plane that is called zeta potential and can be calculated from microelectrophoresis measurements. The principle for microelectrophoresis is that charged particles move in an electric field. Measurements are performed by applying an electrical field to a dilute particle suspension and measuring the direction and velocity of the particle motion. The zeta potential can then be calculated from the electrophoretic mobility[32].

This experimental technique was used to determine the isoelectric point (IEP) of schwertmannite in 100 mM $Na(NO_3)$ medium in Paper 1. The IEP is the pH where net charge at the slip plane is zero, corresponding to zero mobility of particles in an electric field. The zeta potential values in this work have been acquired from dilute suspensions (about 0.1 g dm^{-3}) using a Malvern Zetasizer 4 instrument. The particle size was also determined using this instrument.

2.2.5 X-ray diffraction

Sometimes it is necessary to establish the kind of mineral present in a sample. It can be to confirm that a laboratory synthesis of a mineral is successful or to investigate the minerals present in a field sample. A widely used method to identify minerals is x-ray diffraction, or XRD, where a mineral's "fingerprint" can be detected. This experimental technique was used in Paper 1 to identify the minerals present in the field sample collected at the Kristineberg mine and to study the influence of pH on the rate of transformation of schwertmannite. It was also used in Paper 5 to identify the phases precipitating from AMD at different conditions.

In an XRD measurement the sample is irradiated with monochromatic x-rays. When the x-rays hit the sample a number of events can take place but what is of interest in XRD is the reflection (or scattering) of x-rays from the solid with an angle of reflectance equal to the angle of incidence (θ). If constructive interference occurs between two parallel reflected x-rays, a peak appears in the XRD pattern and the distance d (d-spacing) between reflecting atomic planes can be calculated according to Bragg's law:

$$2d \sin \theta = n\lambda \qquad (2.2)$$

In this way a number of d-spacings are detected. The set of d-spacings and their relative intensities are (almost) unique for each mineral and can be used to identify the sample from tabulated values in the Powder Diffraction File (PDF)[33].

XRD analyses in this work were conducted using Cu Kα radiation and a Bruker D8 Advance instrument. Samples dried at 40°C were scanned from 5 to 90° 2θ with continuous scans at a rate of 1° 2θ min^{-1}. Repeated scans were added until sufficiently good diffractograms were acquired.

2.2.6 X-ray absorption spectroscopy

With x-ray absorption spectroscopy (XAS) it is possible to probe the local environment (the first 2-3 shells of atoms around the absorbing atom) of the element of interest in considerable detail. The main advantage of XAS is that any phase can be studied; gases, liquids, solutions, and solids. Unfortunately, the lighter elements in the periodic table (P and lighter) are technically much more difficult to study. This technique was used to study the adsorption of Cu(II) and Cd(II) to schwertmannite and Cu(II) to goethite (Paper 2).

The principle of XAS analysis is based on the photoelectric effect, i.e. electrons can be emitted if a sample is bombarded with radiation. In XAS, the sample is bombarded with monochromatic x-rays that cause core

electrons to be ejected from the element of interest and the absorption (or fluorescence) by the sample is measured as a function of x-ray energy. Each element has a well-defined threshold energy (binding energy of electron), E_0, that has to be reached before the core electrons are ejected by the x-rays. At this energy the absorption of the incident x-rays increases drastically, the so called "absorption edge". At energies higher than the absorption edge, the absorption slowly decreases. For all compounds other than mono-atomic gases, the decrease in absorption shows oscillations due to interference from photoelectrons backscattered from neighbouring atoms. This region of the spectrum is called extended x-ray absorption fine structure (EXAFS) region and is the region used in this thesis to study the adsorption of Cu(II) and Cd(II) to schwertmannite and goethite.

The acquired spectra undergo what is known as data reduction, which extracts the oscillations due to backscattering. In order to determine how the investigated element coordinate, the acquired data set is compared with a likely model compound where the number of backscattering atoms (N_j) and the distance to the backscatterer (R_j) are known. The parameters defining the scattering are obtained for the model system by computer simulations. The scattering parameters can then be used to obtain N_j and R_j from the investigated spectrum. Further description of XAS theory, techniques and data analysis can be found in the monographs by Teo[34] and Jalilehvand[35]. The use of XAS in coordination chemistry is reviewed by Penner-Hahn[36].

Cu and Cd K-edge EXAFS data were collected in fluorescence mode at the Stanford Synchrotron Radiation Laboratory, California on beam line 4-1. The experimental conditions are further described in Paper 2.

2.2.7 X-ray photoelectron spectroscopy

With x-ray photoelectron spectroscopy, or XPS, it is possible to obtain information about reactions taking place at the mineral surface as XPS analysis is rather surface selective, probing only the first few atomic layers of the surface. XPS can be used to determine elemental composition and also the oxidation state and the functional group of which the element in question is a part. It can in this way be used to follow e.g. redox, sorption and acid/base reactions at the surface. This experimental technique was used in Paper 1 to study the influence of pH on release of SO_4^{2-} from the schwertmannite surface and also to characterise the schwertmannite sample. XPS was also used in Paper 5 to study some of the precipitates formed from AMD.

As with XAS, XPS analysis is based on the photoelectric effect. Due to interactions with the investigated solid, only the electrons excited by x-ray

within the first 5-10 nm of the surface will leave the solid without energy loss. All electrons with a binding energy less than the energy of the x-ray radiation can be emitted but it is only the core electrons that are studied with XPS. The kinetic energy, E_k, of the emitted electrons is measured by an electron spectrometer and the binding energy, E_b (the same as E_0 in XAS), can be calculated according to:

$$E_b = h\nu - E_k - \Phi \quad (2.3)$$

where $h\nu$ is the photon energy of x-rays and Φ is the spectrometer work function (an apparatus constant). Each element has a unique set of E_b and tabulated values for the core electrons can therefore be used to identify elements (Figure 2.2), their oxidation state and functional groups. E_b is affected a few eV by the valence electrons and changes in e.g. oxidation state and coordination cause shifts in E_b. Analysis of the shifts in E_b can thereby be used to follow acid/base reactions and redox reactions while the atomic ratios can be used to study sorption processes[37,38].

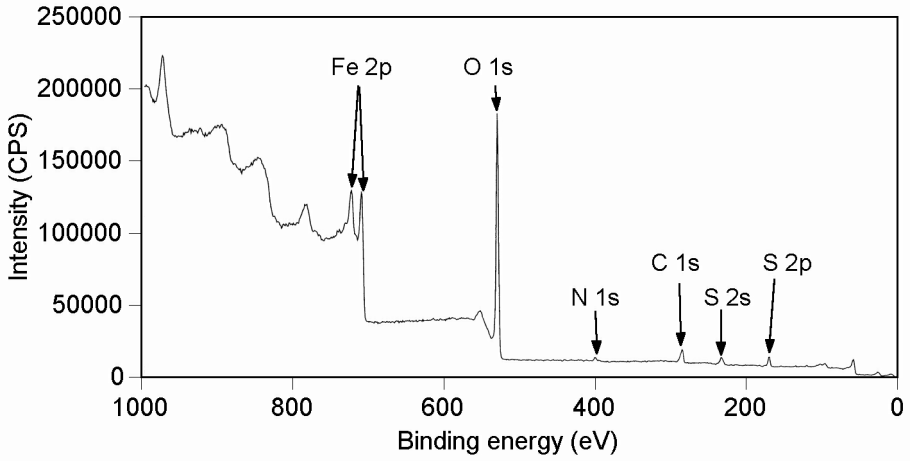

Figure 2.2 XPS wide spectra of Kristineberg schwertmannite with peak assignment.

The instrument used in this work was a Kratos AXIS Ultra electron spectrometer. All measurements in Paper 1 were performed at -160°C to reduce the loss of H_2O from the dried powders. The samples were loaded on the precooled end of a transfer rod within the sample introduction chamber and the pressure was reduced to 10^{-5} Pa. The sample was then transferred to the precooled manipulator where it was kept until a base vacuum of ~$5 \cdot 10^{-7}$ Pa in the analysis chamber was reached. For the XPS analysis in Paper 5 the same conditions were used except that the measurements were performed at room temperature. Wide spectra (pass energy 160 eV) and spectra of

individual photoelectron lines (pass energy 20 eV) C 1s, N 1s, O 1s, Na 1s, Cl 2p, S 2p, Fe 2p, and Zn 2p were acquired using an Al Kα source operated at 225 W. Spectra were processed with Kratos software, and the binding energy scale was referenced to the C 1s line of aliphatic carbon contamination set at 285.0 eV.

2.2.8 Fourier transform infrared spectroscopy

Infrared (IR) spectroscopy is another technique that enables the identification of species formed during chemical reactions. This method utilises the fact that molecules vibrate and the amplitude of the vibration can be increase if the molecule is irradiated with infrared light. If the symmetry of the compound is changed, the vibration may occur at a different wavelength. At certain radiation energy, the so-called vibrational frequency, a molecule absorbs part of the incoming energy, causing different types of vibration, e.g. stretching (ν) and deformation (δ). The type of vibration will depend on the energy of the radiation and the symmetry of the studied compound. The formation and removal of bonds changes the symmetry of the studied compound and a change in symmetry could change the IR spectrum[39,40]. Information from IR spectroscopy is acquired by irradiating a sample and analysing the amount of radiation absorbed at different wavelengths. This method was used to study the speciation of SO_4^{2-} in Paper 1.

IR spectra were collected with a Bruker IFS 66/v FTIR spectrometer equipped with a deuterated triglycine sulphate (DTGS) detector. The samples were analysed with an attenuated total reflectance (ATR) cell with a diamond crystal as the reflecting element. The samples were applied to the diamond surface and a metal lid was placed over the sample and pressed tightly against a rubber gasket. The sample chamber was evacuated to a pressure of 3 mbar to exclude CO_2 and water vapour. 500-1000 scans at a resolution of 4 cm^{-1} were collected over the range 370 to 4000 cm^{-1}. Sample spectra were interpreted after subtracting the spectra for the empty cell and supernatant as required[41].

3 SCHWERTMANNITE

As mentioned in Chapter 1, schwertmannite is potentially a very important mineral forming from AMD where pH values between 3 and 4 are commonly encountered[2]. In this chapter the schwertmannite sample introduced in Section 2.1.1 is described in terms of composition, stability and speciation of SO_4^{2-}. The results are compared to literature information, if available. But first a view of the mineral's history, which is quite interesting in itself, and of where schwertmannite is reported to have been found.

3.1 History and occurrence

Schwertmannite was originally called glockerite after E.F. Glocker, who described the mineral in 1853 from a location in The Czech Republic[42]. In 1975, Fojt[43] published an article were he concluded that glockerite was lepidocrocite and the name glockerite was discredited in 1977[44]. In 1990, Bigham *et al.*[45] described a "poorly crystallized oxyhydroxysulfate of Fe" that in 1992 was approved by the Commission on New Minerals and Mineral Names[46]. The mineral was named schwertmannite in honour of Udo Schwertmann, professor of soil science at the Technical University of Munich. Samples from the location of glockerite was later collected by Schwertmann and Fojt[47] and matched with schwertmannite[2,44]. Schwertmannite has been observed in many places, mainly in areas affected by mining activity and AMD. Schwertmannite has also been observed in areas not affected by mining activity, but the formation is still due to weathering of pyrite[48-50]. It has also been suggested that schwertmannite is a possible mineral at the surface of the planet Mars[51,52] and that it precipitates during Zn extraction in the Zincor process[53].

3.2 Composition and structural features

Ideally, schwertmannite has a Fe/S molar ratio of 8 but the amount of SO_4^{2-} is variable due to adsorbed SO_4^{2-} and is therefore usually described as $Fe_8O_8(OH)_{8-2x}(SO_4)_x \cdot nH_2O$ where $1 \leq x \leq 1.75$[46]. This gives a molar ratio of $8 \leq Fe/S \leq 4.6$, though higher values of x have been reported[54,55] or assumed[11].

The Kristineberg schwertmannite, described in Paper 1, was present as small piles on top of a soil covered tailings impoundment, indicating that the material was formed as a result of oxidation of up-welling groundwater rich in ferrous iron. The elemental analysis of the solid (Table 3.1) showed that Fe and S are the dominating elements with some impurities of mainly C and

Si. The sample has the composition $Fe_8O_8(OH)_{5.02}(SO_4)_{1.49} \cdot 1.05\ H_2O$ with about one third of the SO_4^{2-} adsorbed at the surface. The Fe/S ratio is 5.36, well within the values reported in literature. The Loss On Ignition (LOI), i.e. the weight loss on heating to 1000°C, is high due to loss of SO_3 and H_2O but similar to values previously reported[45,46,54,56]. Drying the sample at 110°C overnight resulted in a weight loss of about 10%. The pore water of the sample contained rather high concentrations of S, Ca and Mg (Table 3.2), the latter two probably originating from liming upstream of the sampling location. Most of the elements in the water phase were reduced by >95% during washing.

Table 3.1 Characterisation of schwertmannite. Elements in μmol g^{-1}, H_2O and LOI in weight-% of dry weight.

Fe	8 700	Na	29	Zn	0.15	Zr	0.034	Mn	<0.46	Nb	<0.06
S	1 600	Mg	11	Ba	0.12	Co	0.006	W	<0.32	Mo	<0.06
C	580	P	6.8	La	0.094	Ni	0.004	Cr	<0.19	Sc	<0.02
Si	340	As	2.8	Pb	0.081	Cd	0.0002	Sn	<0.17	Hg	<0.0002
Al	56	V	0.74	Sr	0.068	N	<35	Cu	<0.16	LOI	35.6
K	37	Ti	0.53	Y	0.056	Ca	<18	Be	<0.07	H_2O	20.7

Table 3.2 Elemental analysis of centrifuged (5000 rpm) pore water from the schwertmannite sample. Concentrations in μM, besides Hg which is in nM.

S	25 800	Al	960	Fe	130	Sr	12	Cd	0.16	As	0.012
Ca	13 000	Si	950	K	100	Ni	7.6	Ba	0.067	Pb	0.008
Mg	10 700	Mn	670	Zn	29	Cu	1.5	Mo	0.047	Hg	0.045
Na	1 050	C	470	Co	15	P	0.97	Cr	0.026		

XPS analyses of the surface region (Table 3.3) show that most of the carbon is present at the surface since Fe/C = 1.5 at the surface and 15 for the bulk sample. The carbon is partly due to contamination by hydrocarbons from air[57] but probably also originates from micro-organisms (bacteria and/or fungi) as some pale, thin "threads" were observed in the material during sampling. That C is found at the surface instead of incorporated into the crystal structure of the schwertmannite also agrees with the assumption that the C comes from air contamination and micro-organisms. At the surface Fe/S = 5.27, which is very close to the value determined from the elemental composition of the bulk phase (Fe/S = 5.36). Fe was found to be in the form of Fe(III) and S in the form of SO_4^{2-}.

Table 3.3 XPS analysis of the schwertmannite surface-region in atomic percent. O and C are also divided into functional groups.

Element	Total								
Fe	21								
O	59	OH	26	SO_4	16	O	10	H_2O	7
S	4								
C	14	C-H	6	C-OH	5	COOH	3		
N	2								

Recently, Yu *et al.*[58] suggested that schwertmannite contains no, or very little, OH^- based on thermoanalysis and gave the alternative formula of $Fe_2O_{3-x}(SO_4)_x \cdot nH_2O$ for schwertmannite, where $0.41 \leq x \leq 0.49$ and $1.51 \leq n \leq 2.81$. However, Cornell and Schwertmann[44] suggested that dehydroxylation of the FeOOH part in schwertmannite merges with adsorbed water loss at low temperature due to the poor crystallinity of schwertmannite. XPS analysis of the surface region of the Kristineberg schwertmannite (Table 3.3) indicates that the sample contained a considerable amount of OH, in contrast to the suggestion by Yu *et al.*[58]. It can be argued that XPS is a surface sensitive method, but it does penetrate down to about 6 nm in this sample (A. Shchukarev, pers. com.). This depth corresponds to about 9% of the total volume if a sphere of 400 nm in diameter is assumed (see below). The OH/Fe ratio (1.24) from XPS analysis is higher than the formula suggests (0.63) but this could be explained by considering protonation of the surface at low pH e.g.:

$$\equiv Fe_3O^{-0.5} + H^+ \rightleftarrows \equiv Fe_3OH^{+0.5}$$

The protonation is supported by zeta potential measurements (Figure 3.1). Even if SO_4^{2-} is adsorbed at the surface at low pH, the zeta potential of the particles is still positive, though half of that of goethite[59]. As pH increases to pH 7, the zeta potential steadily decreases but just above pH 7 a relatively sharp drop in zeta potential occurs and reaches zero around pH 7.2.

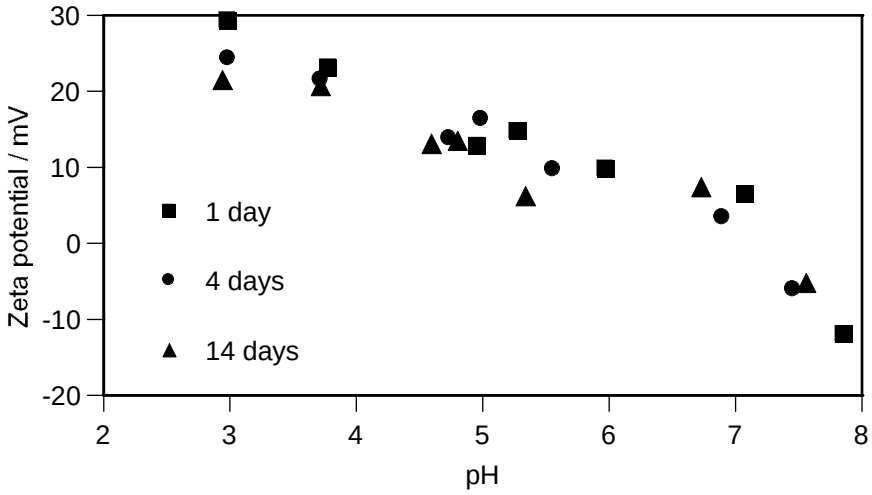

Figure 3.1 The change in zeta potential as a function of pH and time in 0.1 M $NaNO_3$. Initial schwertmannite concentration is 0.1 g dm^{-3}.

The structure of schwertmannite is believed to resemble that of akaganéite (β-$FeO(OH)_{1-x}Cl_x$) which has edge sharing Fe octahedra forming a tunnel-like structure with Cl in the cavities[45] (Figure 3.2).

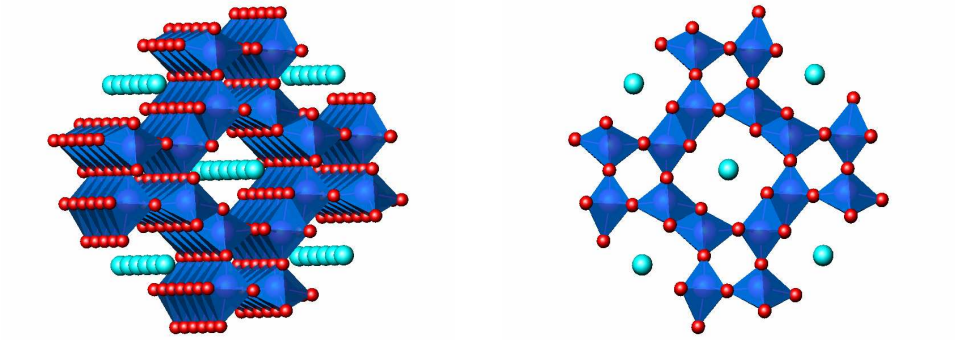

Figure 3.2 The structure of akaganéite, consisting of double chains of edge-sharing $FeO_3(OH)_3$ octahedra. The octahedra comprising the double chain share corners with adjacent chains. Chloride ions neutralise charges in the tunnels. In schwertmannite the Cl^- is replaced by SO_4^{2-} that is suggested to share oxygen with two adjacent Fe-chains.

In schwertmannite, SO_4^{2-} is suggested to replace the Cl^- but due to size restrictions, SO_4^{2-} has to share oxygen with some of the Fe atoms forming a bridging bidentate complex of the type -Fe-O-SO_2-O-Fe- in the tunnels. This leads to distortions in the structure and the poor crystallinity mentioned above[46]. The existence of two different Fe sites is supported by Mössbauer spectroscopy[45,46]. Schwertmannite is suggested to have a primitive

tetragonal unit cell with a = 10.66 Å and c = 6.04 Å[45,46]. The edge sharing Fe octahedra have been confirmed by EXAFS where Fe-Fe distances of 3.03 and 3.37 Å were reported[60], the same values as for goethite.

The poor crystallinity is visible in the XRD pattern, where eight characteristic broad peaks appear[13,46,48]. Schwertmannite was detected in the Kristineberg sample using XRD (Figure 3.3).

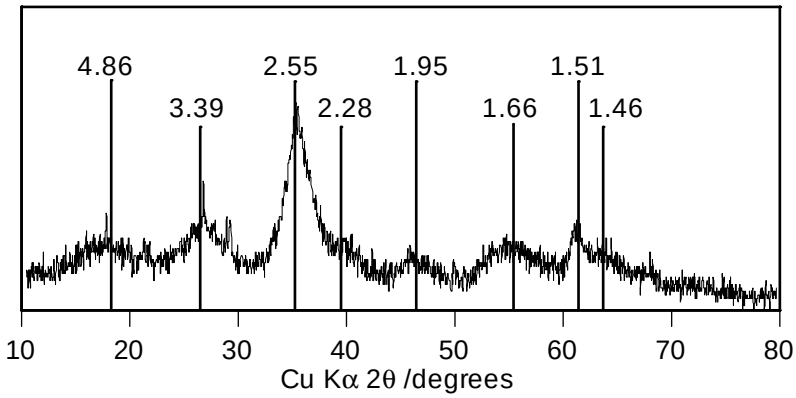

Figure 3.3 XRD of schwertmannite from the Kristineberg mine. The d-spacings (Å) for schwertmannite (PDF 47-1775) are included for reference.

In mixed-mineral samples, the low-intensity XRD peaks of schwertmannite can often be hidden by more intense peaks from more crystalline minerals such as goethite. The technique of differential XRD (DXRD) can then be used to identify schwertmannite[61]. With this technique, an XRD pattern is recorded followed by partial extraction of the mineral mixture in acidic oxalate solutions (pH 3, 0.2 M, in darkness)[62] whereafter a new XRD pattern is recorded. As low-crystallinity iron oxides such as schwertmannite are readily dissolved in acidic oxalate solutions[2] the difference between the two spectra will ideally identify the dissolved phase. Dold[63] has recently suggested that an extraction time of 15 min would be sufficient if schwertmannite were to be detected using DXRD, whereas 60 min is more appropriate if the entire schwertmannite sample is to be dissolved. DXRD was not performed with the Kristineberg schwertmannite but the sample was totally dissolved in acidic oxalate solution within 45 min, confirming the low crystallinity.

Schwertmannite forms characteristic pincushion-like aggregates, usually about 200-500 nm in diameter, leading to a rather high surface area of about 100-300 m^2 g^{-1} [13,44,46]. The pincushion morphology is not always detectable, especially if samples are taken from consolidated sediments or

surface crusts[2]. When the Kristineberg schwertmannite was investigated with scanning electron microscopy (SEM, Figure 3.4), it was clear that the individual particles were almost spherical, had a diameter of about 300-500 nm, and formed larger aggregates. The pincushion morphology could not be detected with SEM, possibly due to the washing, centrifugation and grinding of the sample. The particles look very similar to the schwertmannite particles described by Kawano and Tomita[50]. Even if the individual particles are relatively small, the surface area was rather low, 43 $m^2\ g^{-1}$, for the washed sample. This low value is probably an artefact due to adsorbed SO_4^{2-} as discussed in Section 3.4 and Paper 1.

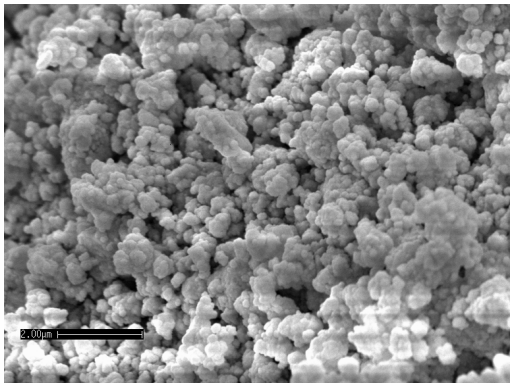

Figure 3.4 SEM picture of gold-coated Kristineberg schwertmannite. Scale bar (2 µm) in the bottom left corner.

Schwertmannite has been studied with infrared techniques by a number of authors[12,45,46,48,64-67] and also with Raman spectroscopy[68]. The bands and their assignments are compiled in Table 3.4. Most studies have been conducted by diluting a dried sample in KBr but Peak *et al*.[66] studied the frequency region between 900 and 1300 cm^{-1} of a suspension of schwertmannite that was allowed to dry on the ATR-IR cell and compared this with a KBr spectrum. The IR spectrum of schwertmannite is characterised by absorption bands associated with H_2O, SO_4^{2-} and Fe(III).

Table 3.4 IR bands for schwertmannite with band assignments, compiled from the references above.

Band	Wavenumber /cm^{-1}
ν(OH)	3185-3500
$\delta(H_2O)$	1620-1650
COOH impurities	~1400
$\nu_3(SO_4)$ shoulder	1170-1186
$\nu_3(SO_4)$ most intense	1124-1142
$\nu_3(SO_4)$ shoulder	1035-1070
$\nu_1(SO_4)$	970-981
δ(OH) broad shoulder	800-900
$\nu_3(FeO,OH)_6$	~700
$\nu_4(SO_4)$	603-618

Besides the bands in Table 3.4, a band at 1202-1212 cm^{-1} has been reported but Peak *et al.*[66] claim that this is an artefact due to drying and dilution of KBr as this band was not visible when the sample was run in ATR mode. A possible weak $\nu_2(SO_4)$ at 465 cm^{-1} has also been reported. The ATR-IR spectrum for the dry Kristineberg schwertmannite is presented in Figure 3.5. The bands from water are clearly visible at 3000-3500 and 1635 cm^{-1}. The $\nu_3(SO_4)$ is centred at 1121 cm^{-1} with shoulders at 1185 and 1057 cm^{-1} and the $\nu_1(SO_4)$ at 976 cm^{-1}. The shoulder between 800-900 cm^{-1} along with the bands at 701 and 605 cm^{-1} are also clearly visible. A band of possible extra interest is the one assigned to $\nu_4(SO_4)$. Bigham *et al.*[45] synthesised a SO_4^{2-}-free analogue to schwertmannite and then allowed SO_4^{2-} to adsorb. The ν_4 band was absent in this sample and the authors pointed out that this could be a way to distinguish between structural and adsorbed SO_4^{2-}.

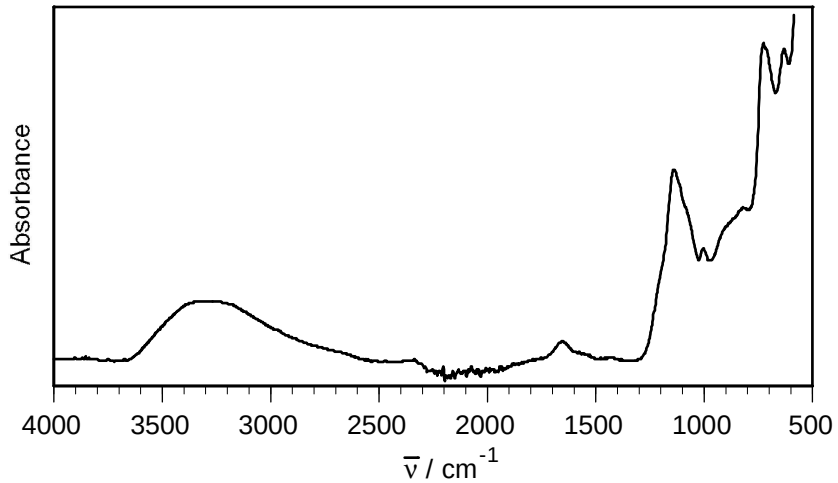

Figure 3.5 ATR-IR spectrum of Kristineberg schwertmannite, dried at 40°C.

3.3 Stability and transformation

As the poor crystallinity of schwertmannite might suggest, the mineral is not very stable and transforms into goethite over time as shown by Bigham *et al.*[14], when a synthetic sample was totally transformed after 543 days in distilled water, accompanied by a pH drop from 3.9 to 2.4. The authors suggested that schwertmannite was transformed according to Equation (3.1):

$$Fe_8O_8(OH)_6(SO_4)_{(s)} + 2\ OH^- \rightarrow 8\ FeOOH(s) + SO_4^{2-} \qquad (3.1)$$

The transformation is supported by the findings of Peine *et al.*[69] for an acidic lake where schwertmannite was suggested to precipitate, sediment and transform to goethite in the sediments. The transformation of schwertmannite is also evident in that goethite is often associated with findings of schwertmannite[12,14,54,70-73]. Kawano and Tomita[50] suggested that schwertmannite was transformed into jarosite at low pH (<2.6) and high SO_4^{2-} concentration (>60 mM).

The stability of the Kristineberg schwertmannite was studied at two pH values, 6 and 9, from 6 h up to 514 days at 25°C. Two samples were also left in the original pore water at 4 and 25°C. The XRD analysis of the solids at pH 6 and 9 showed a gradual transformation of schwertmannite into goethite (Figure 3.6).

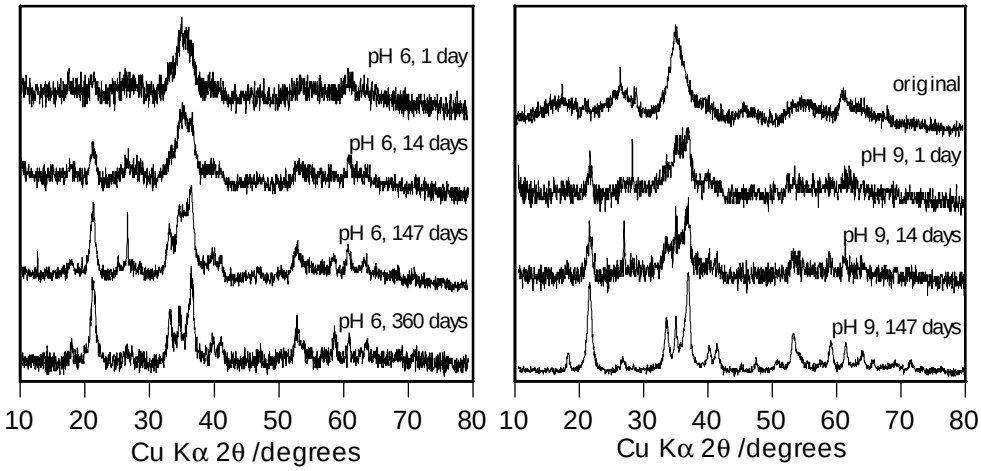

Figure 3.6 XRD spectra for schwertmannite at different pH values and after different ageing time at 25°C. The spectrum for the original schwertmannite sample is included for comparison. The spectrum labelled "pH 9, 147 days" shows "pure" goethite. Initial schwertmannite concentration is 50 g dm^{-3}.

As can be expected from Equation 3.1, the transformation is favoured by an increase in pH. According to the OH^- consumption the sample at pH 9 was

completely transformed after 187 days, only 2.4% of the total amount of OH^- was added during the last 327 days. At pH 6 the consumption of OH^- continued for the entire period, 26% of the total amount of OH^- was added between day 187 and 514, indicating that the transformation was not complete during the time frame of the study.

Goethite and possibly traces of H-jarosite were detected in the sample that was left in the original pore water and stored at 25°C during 1362 days (Figure 3.7), although the transformation did not seem to be complete. The pH had also dropped from 3.0 to about 1.9. The pH drop can partly be attributed to oxidation of residual Fe(II) left in solution followed by precipitation but mainly to the transformation to goethite and possibly due to evaporation. For the sample stored at 4°C, no transformation was detected even after 1752 days (Figure 3.7) though gypsum was detected. The formation of gypsum is expected as the pore water was slightly supersaturated with respect to this mineral at the time of the sampling (Table 3.2). pH in the pore water was also almost unchanged, pH 2.95 was measured after 1752 days which also indicates that no transformation occurred.

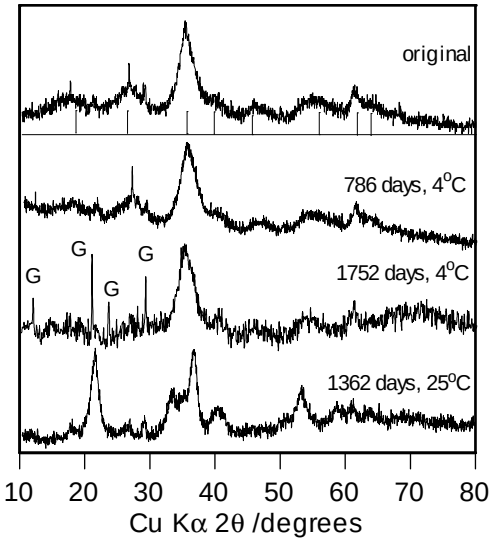

Figure 3.7 XRD spectra for schwertmannite stored in the original pore water after different ageing times at 4 or 25°C. The spectrum for the original schwertmannite sample is included for comparison. The peaks labelled G show gypsum.

These results indicate that schwertmannite can be relatively stable at low pH and temperature and high SO_4^{2-} concentration. The temperature dependence is supported by the fact that autoclaving schwertmannite is suggested to complete the transformation in 20 min[74].

As pointed out by Bigham *et al.*[14], the calculation of a solubility product constant is probably rather impractical due to transformation to goethite, the existence of both structural and adsorbed SO_4^{2-} and the variable composition. The constant may serve a purpose in estimating whether or not schwertmannite is likely to precipitate. For the dissolution reaction in Equation (3.2):

$$Fe_8O_8(OH)_{8-2x}(SO_4)_{x(s)} + (24-2x)\ H^+_{(aq)} \rightleftarrows 8\ Fe^{3+}_{(aq)} + x\ SO_4^{2-}{}_{(aq)} + (16-2x)\ H_2O_{(l)} \quad (3.2)$$

there are several values given for log K in the literature. Bigham *et al.*[14] calculate a value of log K = 18.0 ± 2.5 assuming equilibrium in the waters where the samples were collected. Yu *et al.*[54] calculated a value of log K = 10.5 ± 2.5 assuming that the water was supersaturated with respect to schwertmannite. Yu *et al.*[75] have also suggested that log K for the reaction might be as low as 0. Zänker *et al.*[60] found that a value of log K < 8.9 fitted their results with simultaneous precipitation of H-jarosite and schwertmannite. For a schwertmannite with the composition of $Fe_8O_8(OH)_{5.9}(SO_4)_{1.05}$, Kawano and Tomita[50] reported a log K = 7.06. For synthetic samples Yu *et al.*[58] reported a value of log K = 2.01 ± 0.30 for their alternative schwertmannite formula, corresponding to log K = 7.88 for the formula from Bigham *et al.*[14]. Yu *et al.*[58] also reported that the log K value was dependent on the SO_4^{2-} content. The differences between the different constants are rather large but this is at least partly due to uncertainty in pH as 1 pH unit changes the value of K by up to 10^{22}. Attempts were made to calculate a dissolution constant for the Kristineberg schwertmannite from the concentrations in the original pore water but were not meaningful due to uncertainties in pH and concentrations of Fe^{2+} and Fe^{3+}.

Schwertmannite not only transforms in suspension but also upon heating as H_2O and, at high temperature, SO_3 are lost from the schwertmannite structure. Barham[64] reported formation of hematite (α-Fe_2O_3) or jarosites when schwertmannite was heated to 200°C. Kim and Kim[55] suggested that schwertmannite is thermally decomposed around 140°C due to dehydration. Further heating results in further water loss and a gradual transformation to more well-crystalline hematite and $Fe_2(SO_4)_3$ followed by the release of SO_3 at 630-680°C when $Fe_2(SO_4)_3$ transforms into hematite[45,54]. However, Mazzetti and Thistlethwaite[68] could not detect $Fe_2(SO_4)_3$ when they heated

schwertmannite with a laser beam using Raman spectroscopy and instead suggested that maghemite (γ-Fe_2O_3) was formed before transformation to hematite.

3.4 Sulphate speciation and surface area

The validity of Equation (3.1) was also confirmed by analysis of aqueous SO_4^{2-} concentration and consumed OH^-. The amounts of released SO_4^{2-} and consumed OH^- differed by less than 50 μmol g^{-1} (3% of total the SO_4^{2-}-content) for most of the samples kept at pH 6 and 9 (Figure 3.8 a).

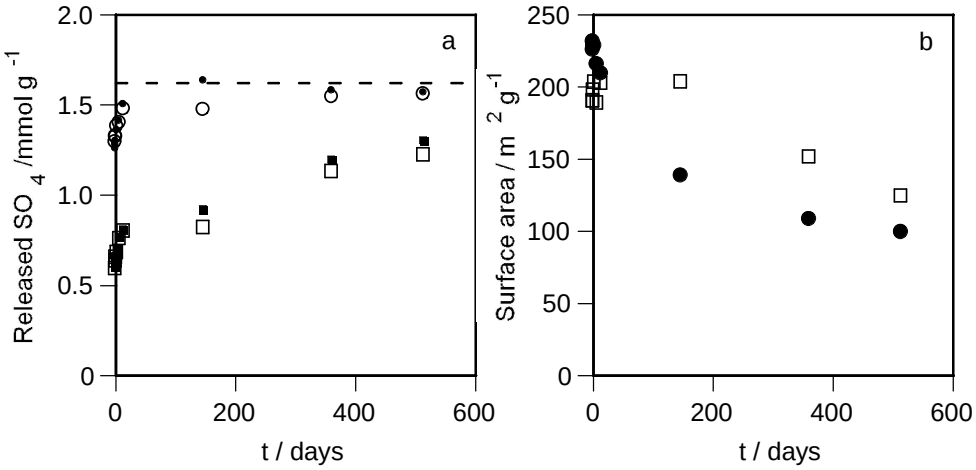

Figure 3.8 a) Release of SO_4^{2-} as a function of time at pH 9 (circles) and pH 6 (squares). Filled symbols are calculated from aqueous SO_4^{2-} concentration and open symbols from consumed OH^-. The total amount of SO_4^{2-} in the solid (1.62 mmol g^{-1}) is indicated by a dashed line. b) Change in specific surface area as a function of time for schwertmannite at pH 6 (□) and pH 9 (●). Initial schwertmannite concentration is 50 g dm^{-3}.

The release of SO_4^{2-} was also accompanied by a 5-fold increase in surface area after only 6 h (Figure 3.8 b). The low surface area (43 m^2 g^{-1}) of the original sample seems to arise from adsorbed SO_4^{2-} as the surface area increases as the SO_4^{2-} is released from the solid. One possible explanation is that adsorbed SO_4^{2-} facilitates aggregation of the particles while drying and thereby reduces the surface area available for the N_2 gas in the BET measurement, as is the case for PO_4^{3-} adsorbed to goethite[76]. The surface area of the samples decreases with time which is probably an effect of both a change in density from schwertmannite (3.75-3.90 g cm^{-3})[45] to goethite (4.26 g cm^{-3})[44] and a slight increase in particle size with time (Oswald ripening). The slower decrease in surface area at pH 6 can possibly be attributed to the slower conversion rate at this pH and to adsorption of

SO_4^{2-}. Sulphate and other ions are known to retard crystal growth[44] and at pH 6 it can be expected that more SO_4^{2-} is adsorbed at the surface compared to pH 9[77].

The dried solids were imaged with SEM. In Figure 3.9 a selection of SEM images are shown. As can be seen, the goethite formed retains the original, almost spherical shape of schwertmannite and the individual particles do not seem to change size. This supports the suggestions that the change in surface area is mainly due to the extent of aggregation and also the change in density during transformation from schwertmannite to goethite. For the original sample, with low surface area, the spheres seem to be cemented together whereas the spheres are more clearly defined in the samples with high surface area. When scanning through the samples at low magnification, the samples with the highest surface area were found to have a low degree of large aggregates. However, this could potentially be an artefact of grinding.

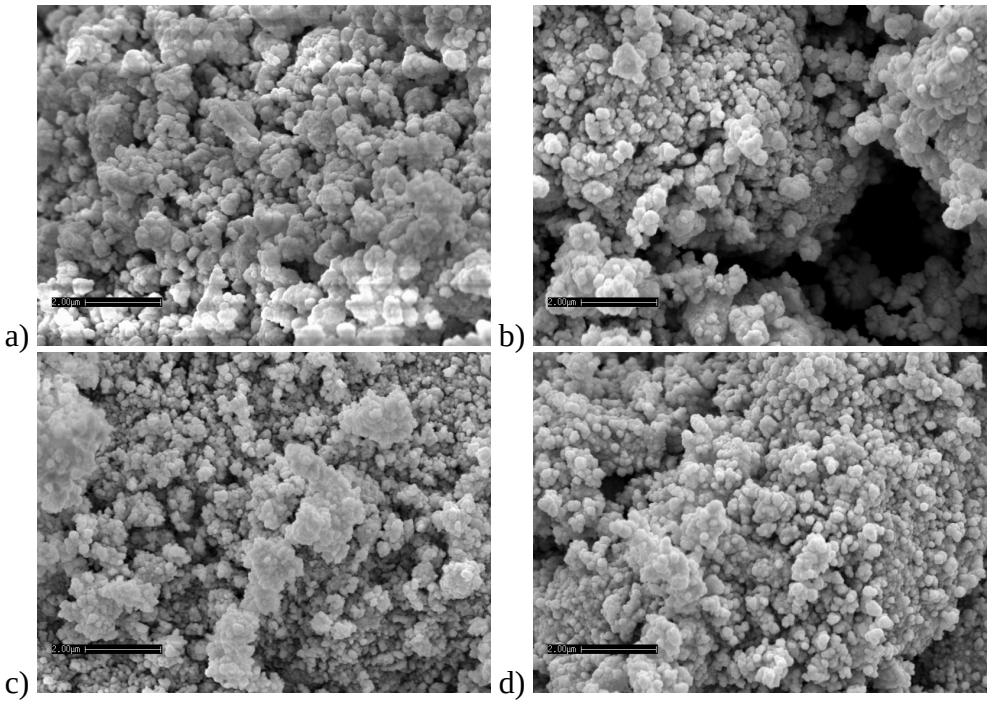

Figure 3.9 SEM pictures of Kristineberg schwertmannite stored at different pH values and after different ageing time: a) original sample, b) pH 6, 6 h, c) pH 9, 514 days, d) original pore water 1362 days at 25°C. Scale bar (2 μm) in the bottom left corner.

Besides aggregation, there are other possible explanations for the initial low surface area of the schwertmannite. The lack of pin-cushion

morphology is one, as the needles provide a large surface area and little weight, but that does not explain why the surface area increases as pH increases. Another possibility is partial dissolution of schwertmannite particles as that would increase the surface/volume ratio. However, no major change in size could be detected in the SEM investigation or in dynamic light scattering measurements. An increase in surface area from 42.9 to 200 $m^2 g^{-1}$ (about 5 times) would require a decrease in particle radius to about 1/5 of the original radius and that is clearly not the case for the individual particles. Less aggregation is a more likely explanation than dissolution as less aggregation could easily decrease the effective particle radius to 1/5 of the original value during the release of the individual particles from the aggregate.

Goethite synthesised in the laboratory forms needle-shaped crystals that are about 100-2000 nm long[59] depending on the method used. As can be seen in Figure 3.9 there are no goethite-needles visible and no needles were detected when scanning through the samples which is in contrast to the findings of Bigham *et al*.[14].

The described study at pH 6 and 9 (Paper 1) indicated that the acid-base properties of schwertmannite were closely linked to the release of SO_4^{2-}. As might be expected from Figure 3.8a, titrations of schwertmannite were not very successful due to the continuous release of SO_4^{2-} and consumption of OH^-. Instead, the pH-stat technique was employed with pH fixed at 3, 4, 5, 6, 7, 8 or 9 during 24 h. The release of SO_4^{2-} was again almost perfectly matched by the consumption of OH^-, showing that two OH^- were consumed for each SO_4^{2-} released, and was linear for the entire pH-range studied (Figure 3.10). This is in contrast to desorption of SO_4^{2-} from e.g. goethite[77]. Linear release of SO_4^{2-} with pH has been reported by Rose and co-workers[78,79] for AMD precipitates though schwertmannite was not identified. Lintnerová and Šefcíková[80] have recently described the linear release from field samples of schwertmannite and a mixture of schwertmannite and jarosite.

As also can be seen in Figure 3.10, the surface area increased almost linearly with pH up to pH 7 after 24 h equilibration, where a fairly constant value of about 225 $m^2 g^{-1}$ was achieved. This result further supports the assumption that SO_4^{2-} in some way bridges particles together when drying as the surface area increases when the solid has been re-suspended in water and more SO_4^{2-} is released and removed from the solid. The value of 225 $m^2 g^{-1}$ is therefore assumed to represent the true specific surface area. Since drying and de-gassing the samples for surface area analyses reduced the weight by 10%, the surface area has correspondingly been adjusted by 10%

to 200 m^2 g^{-1}. This value is used in the rest of the calculations as representing the specific surface area of the original sample.

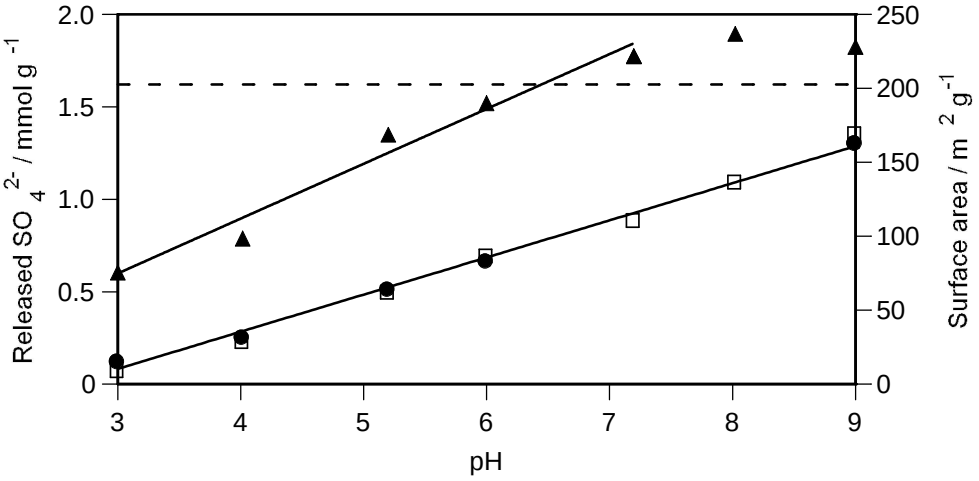

Figure 3.10 The release of SO_4^{2-} calculated from aqueous SO_4^{2-} concentration (●) or OH^- consumption (□) and change in specific surface area (▲) as a function of pH during 24 h equilibration. Initial schwertmannite concentration is 50 g dm^{-3}. The total amount of SO_4^{2-} in the solid (1.62 mmol g^{-1}) is indicated by a dashed line. The equation for the regression lines are:
Released SO_4^{2-} (in mmol g^{-1}) = 0.201 pH - 0.528, R^2 = 0.996
Specific surface area (in m^2 g^{-1}) = 37.07 pH - 37.3, R^2 = 0.972

As mentioned in Section 3.2, schwertmannite is believed to have SO_4^{2-} both in the bulk structure and adsorbed at the surface. In order to study the SO_4^{2-} speciation in more detail, ATR-FTIR spectra of four suspensions at pH 3.0, 4.2, 5.0, and 5.9 were recorded (Paper 1). The frequency region of interest is between 900 and 1300 cm^{-1} where the stretching modes of the S-O bonds show characteristic absorption bands. The undisturbed SO_4^{2-} tetrahedron displays one strong band (ν_3) in this region but when distorted this band is split and an additional stretching mode (ν_1) becomes IR active[40]. As expected from the proposed schwertmannite structure with SO_4^{2-} bonded to Fe in the tunnel structure[45,46], the spectra of schwertmannite display the characteristics of distorted SO_4^{2-} as discussed in Section 3.2. The spectra are very similar to the ATR spectra published by Peak *et al.*[66]. By closer inspection of the ν_3 bands, pH-dependent changes are detected which indicate that SO_4^{2-} speciation varies in the investigated pH interval. The variation is ascribed to adsorbed SO_4^{2-} as the IR characteristics of bulk SO_4^{2-} should be indifferent to pH changes. In order to deconvolute the different contributions to the IR spectra and to study the

adsorbed SO_4^{2-} in more detail, a spectral subtraction technique was used. In the subtraction procedure the end-point spectra at pH 3.0 and 5.9 were subtracted from the remaining three, respectively. In the resulting spectra (Figure 3.11), two surface species can clearly be distinguished which are very similar to the SO_4^{2-} surface complexes on hematite and goethite[66,81]. The existence of two surface complexes on schwertmannite is further corroborated by 2D IR spectroscopy (Paper 1). The surface complex increasing in importance with increasing pH shows features of an almost undistorted SO_4^{2-} with little splitting of ν_3 and a very weak ν_1[40] (Figure 3.11a), and indicates a weak and electrostatic interaction with the surface in an outer sphere mode. Peak *et al.*[66] suggested that this outer sphere SO_4^{2-} is located in the tunnel structure of schwertmannite as a counter ion, though Bigham and co-workers[45,46] suggested that the SO_4^{2-} in the bulk structure should be coordinated in a bidentate mode due to size restrictions. The results presented here suggest that the outer sphere SO_4^{2-} is a surface complex. The other surface complex, predominating at low pH, displays a split ν_3 and an intense ν_1 and is thus significantly distorted which implies a comparatively strong interaction with the surface (Figure 3.11b). In the case of previously investigated iron oxides the structure of this complex has been discussed in the literature[66,81] but still awaits a definitive structural assignment. Nevertheless, the IR data presented here indicate a strong resemblance at the molecular level between SO_4^{2-} surface complexes on schwertmannite and those on other iron oxides.

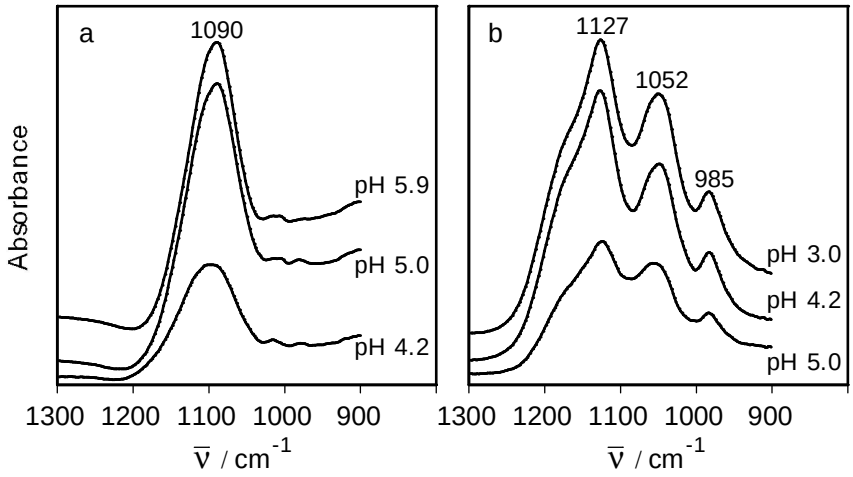

Figure 3.11 Resulting ATR-FTIR spectra after subtraction of a) pH 3.0 and b) pH 5.9 spectra.

4 NOM SAMPLES

As mentioned in Section 1.4, NOM contains functional groups which give NOM acid/base properties and the ability to form complexes with metal ions and surfaces. In this chapter, the elemental composition and the acid-base properties of the collected NOM samples are described. Ideally a NOM sample from the Kristineberg area should have been investigated. Such a sample was collected and concentrated and the C concentration was fairly high; 30 mg C dm^{-3}. The concentration of other elements was however also very high, the Zn concentration (>20 μM in the concentrate) was even higher than some of the concentrations used in Chapter 5 where the metal adsorption to schwertmannite is described. This could have severe implications for the interpretation of titration data as metal ions form complexes with NOM[82]. It was therefore decided to use NOM from a less polluted area. A concern might be that NOM differs between sampling sites but the decision was justified by results from Köhler *et al*.[83], which showed that the acid-base properties of 700 lake and 200 river samples from Sweden were remarkably similar.

4.1 Elemental composition

The April 1999 NOM sample (Paper 3) was collected when the snow and ice had just started to melt and this is evident in that the concentration in this sample (Table 4.1) is significantly lower than in the January 1998 NOM sample (Paper 4), 12 and 37 mg C dm^{-3}, respectively. The 1998 sample had a strong smell of H_2S when sampling but not after the freezing out procedure. The pH values of sampled waters were 4.05 (1998) and 4.33 (1999). After the freezing out procedure the C concentration had increased to 251 and 58 mg C dm^{-3} for the 1998 and 1999 samples, respectively.

The advantage with the freezing out method is that it is a process that occurs naturally and no chemicals are added that may affect the composition of the organic matter. Any reactions taking place during e.g. a pH change can be expected to occur in nature. Extraction of humic acids according to the International Humic Substance Society (IHSS) involves treatments at pH 1 and 11[84] and this treatment can quite possibly change both the structure and acid-base properties of the sample. The drawback with the freezing out procedure is that not only NOM is concentrated but also all other elements, although their concentrations are low compared to the C concentration (Table 4.1).

Table 4.1 Analysis of dissolved elements in the two concentrated NOM samples.

Element	1998	1999	unit	Element	1998	1999	unit
DOC	20.9	4.83	mM	Sr	470	85	nM
Si	580	250	μM	P	420	700	nM
Na	310	150	μM	Ba	130	36	nM
Cl	190	49	μM	Cu	91	34	nM
Ca	170	32	μM	Ni	66	13	nM
Mg	110	22	μM	As	62	10	nM
S	97	71	μM	Pb	41	8.7	nM
K	70	25	μM	Cr	40	13	nM
Fe	61	14	μM	Co	9.8	2.3	nM
Al	19	3.7	μM	Mo	5.4	0.12	nM
Zn	920	180	nM	Cd	3.7	0.74	nM
Mn	920	280	nM	Hg	0.050	0.070	nM

4.2 Acid-base properties

The acid/base properties of the two samples were studied with potentiometric titrations (Section 2.2.2). Both samples had a weak acidity; 300 and 77 μM for the 1998 and 1999 sample, respectively. The buffering at pH<6 was assumed to be from carboxylic groups in NOM and these were treated as a diprotic acid (H_2A). The pK_a-values assigned to carboxylic groups for the two samples are presented in Table 4.2 where they also are extrapolated to zero *I* using the Davies equation[85]. For the 1999 sample the pK_a-values at different *I* are in reasonably good agreement between different *I* considering the experimental difficulties, especially the low total concentration of carboxylate groups. The pK_a-values are within the range reported by Lövgren *et al.*[86] for NOM from this site, except for pK_{a2} for the 1998 sample, which is slightly less acidic. The concentration of H_2A was 0.91 and 0.20 mM for the 1998 and 1999 samples, respectively, corresponding to a so-called site density of 7.25 and 6.90 μekv $(mg\ C)^{-1}$.

Table 4.2 pK_a values for the two NOM samples and extrapolation to zero (0) ionic strength using the Davies equation.

	Sample 1998				Sample 1999			
***I* (M)**	**pK_{a1}**	**pK_{a2}**	**pK_{a1}^0**	**pK_{a2}^0**	**pK_{a1}**	**pK_{a2}**	**pK_{a1}^0**	**pK_{a2}^0**
0.020					3.52	5.11	3.69	5.39
0.100	3.79	5.38	4.08	5.88	3.13	4.90	3.42	5.40
0.600					3.41	4.74	3.77	5.35
Average							3.63	5.38

In Paper 4, this simple acid-base model is compared for the 1998 sample with two other acid-base models for humic substances, WHAM V[87] and a

triprotic model[88]. The evaluation shows that all three models can predict pH in natural waters quite accurately provided some adjustments are made. For the 1998 sample the site density of the carboxylic groups is too low, resulting in a predicted pH value that is higher than measured pH (Paper 4, Figure 3a). The addition of "strong carboxylic acids" corresponding to 1.35 μeq (mg C)$^{-1}$ (340 μM) makes the model more accurate in predicting pH values (Paper 4, Figure 3b). The total carboxylic site density is then 8.6 μeq (mg C)$^{-1}$, the same values as for the triprotic model[88].

In Paper 4 a pK_a-value of 8.50 was assigned to phenolic groups. Whether this value corresponds to phenolic groups only might be discussed. Titration data showed that true equilibrium was not achieved above pH 6 for either of the two NOM samples. For the 1999 sample the volume of added base and equilibrium time were varied to study the influence of these parameters on the buffering response. At pH>7 the results obtained were strongly dependent on these two parameters. As NOM is formed from degraded plant material it is interesting to note that a similar kind of drift above pH 6 is also reported for titrations of wood fibres[89]. The drift in titrations of NOM at pH>6 has been suggested to be due to fragmentation of NOM[90]. If indeed this is the case, the drift in pH above pH 6 is not likely to be visible in a sample treated at pH 11 and will inevitably underestimate the buffering capacity of the organic material at pH>7. The inclusion of a high "phenolic" pK_a makes the adjusted model accurate even at circumneutral pH, compared to the triprotic model by Köhler *et al*.[88] that slightly overestimates pH at pH>6.5 due to lack of buffering capacity.

5 NATURAL ATTENUATION BY SCHWERTMANNITE

Utilising adsorption processes is a possible way to decrease the contamination of metal ions and oxyanions from mine waste. As schwertmannite is often found in association with AMD, the potential of this mineral should be investigated. There is however rather little information regarding metal adsorption to schwertmannite. Webster *et al*.[91] have studied the pH dependence of adsorption of Cd(II), Cu(II), Pb(II) and Zn(II) to a synthetic schwertmannite and compared this with the adsorption to 2-line ferrihydrite and a goethite-bearing AMD precipitate. Unfortunately it is not possible to directly compare the adsorption for the different metals as the concentration scale is in mg metal kg^{-1}. Swedlund and Webster[92] have also tried to model the adsorption of Cu(II) and Zn(II) to schwertmannite using ferrihydrite with adsorbed SO_4^{2-} as a model system. Randall and co-workers[93,94] have investigated Cd(II) adsorption to schwertmannite using EXAFS spectroscopy at pH 6.5 and concluded that Cd(II) formed an inner-sphere complex at the schwertmannite surface, very similar to their results for Cd(II) adsorption on akaganéite. In contrast to Cd(II), U(VI) is suggested to form a ternary type B surface complex ($\equiv$Fe-SO_4-UO_2) at pH 4.2[95]. U(VI) binds to either one or two SO_4^{2-} at the surface of schwertmannite forming a monodentate or a bidentate bridging complex in 10 mM Na_2SO_4 medium. In 10 mM $NaClO_4$ medium the SO_4^{2-} is displaced from the surface and U(VI) forms a bidentate mononuclear inner sphere complex ($\equiv$Fe-$(O)_2$-UO_2).

Besides metal ions, AMD might contain relatively high concentrations of toxic oxyanions such as arsenate (AsO_4^{3-}). The oxyanions are negatively charged and the adsorption of these therefore decreases with increasing pH (i.e. decreasing positive surface charge), in contrast to the adsorption of positively charged metal ions. The oxyanions will also compete with SO_4^{2-} for available surface sites and possibly also for sites in the tunnel structure of schwertmannite. The competition for surface sites between anions might affect the formation of ternary complexes with metal ions. A few studies have been conducted where the adsorption of oxyanions to schwertmannite has been investigated. Carlson *et al*.[96] studied the effect of AsO_4^{3-} on schwertmannite precipitation and adsorption of AsO_4^{3-} to the surface at pH 3 and found that 60% of the SO_4^{2-} could be released in the presence of AsO_4^{3-}. This is similar to the amount replaced by Cl^- (Paper 1). The authors suggested that FeOH-As might be forming as a coprecipitate or as a surface phase, as suggested from ferrihydrite data. The AsO_4^{3-} content was in the same range as for schwertmannite formed by coprecipitation from mixed

sulphate/arsenate solutions, indicating that not only surface SO_4^{2-} was replaced by AsO_4^{3-}. This was also supported by their XRD data. However, Waychunas *et al*.[97] suggested from EXAFS data that AsO_4^{3-} mainly adsorbs to the surface, even though they examined synthetic samples with varying amounts of AsO_4^{3-} replacing SO_4^{2-} during synthesis. Arsenate was suggested to destabilise the structure and poison growth. Fukushi and co-workers[98,99] found that schwertmannite could adsorb arsenate up to 0.58 mmol g^{-1} which also stabilised schwertmannite so that the transformation to goethite did not take place; the more arsenate the slower transformation. Selenate (SeO_4^{2-}) does not affect the structure and was reported to substitute directly for SO_4^{2-}, both in the structure and at the surface[97]. Barham[64] conducted an IR study where SO_4^{2-} was replaced with oxalate ($C_2O_4^{2-}$), chromate (CrO_4^{2-}) and carbonate (CO_3^{2-}). The replacement was reported to be reversible.

5.1 Batch adsorption

The adsorption of Cd(II), Cu(II), Pb(II), and Zn(II) to schwertmannite as a function of pH was studied with batch sorption experiments with varying adsorbate/adsorbent ratios. The adsorption showed a typical cation pattern, i.e. the adsorption increased with an increase in pH (Figure 5.1). Cu(II) and Pb(II) start adsorbing around pH 3-3.5, followed by Zn(II) at about pH 4 and then Cd(II) at about pH 5. The adsorption increases from 0 to 100% within about 2 pH units. A comparison with published results is somewhat difficult as Webster *et al*.[91] and Swedlund and Webster[92] have used different solid concentrations for different experiments. They also reported their results in metal/Fe ratios and had a different specific surface area of their schwertmannite. Though the general trend agrees with their results, it seems the schwertmannite used in this study has a somewhat higher affinity for the different metals. However, this could be due to differences in solid concentrations and specific surface area.

As can be seen in Figure 5.1, the adsorption of Cu(II) and Pb(II) is very similar and to elucidate which metal ion adsorbs strongest, a competitive experiment was performed where both metal ions were added to a schwertmannite suspension. No clear difference could be detected (Figure 5.2) but it seems as if slightly more Pb(II) than Cu(II) adsorbs at pH<5.2 and slightly less Pb(II) than Cu(II) at pH>5.4.

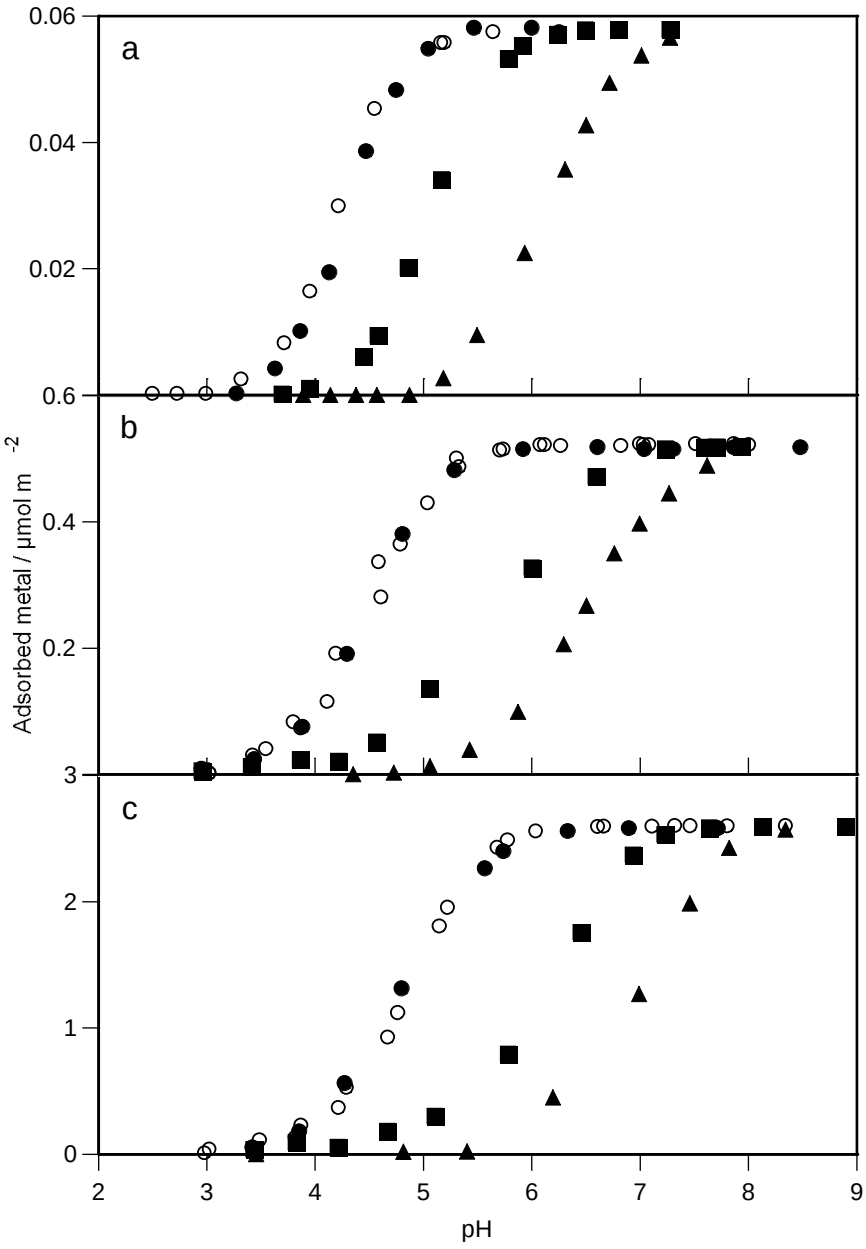

Figure 5.1 Adsorption of Cu(II) (○), Pb(II) (●), Zn(II) (■) and Cd(II) (▲) to schwertmannite as a function of pH with metal/schwertmannite ratios of a) 0.057, b) 0.52 and c) 2.6 µmol m^{-2}. Note the different scales on the y-axes. Initial schwertmannite concentration = 1 g dm^{-3} with a specific surface area of 200 m^2 g^{-1}.

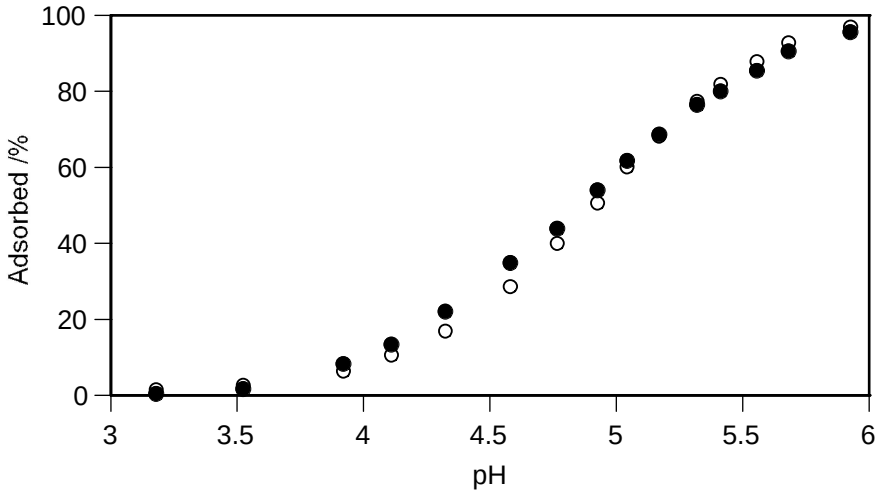

Figure 5.2 Competitive adsorption of Cu(II) (○) and Pb(II) (●) as a function of pH with individual metal/schwertmannite ratios of 2.20 µmol m^{-2}. Initial schwertmannite concentration = 1 g dm^{-3} with a specific surface area of 200 m^2 g^{-1}.

As schwertmannite transforms into goethite, it is of interest to compare the results with the adsorption to goethite. For goethite the trends are slightly different with Cu(II) adsorbing at the lowest pH followed by Pb(II), Zn(II) and then Cd(II) (Figure 5.3).

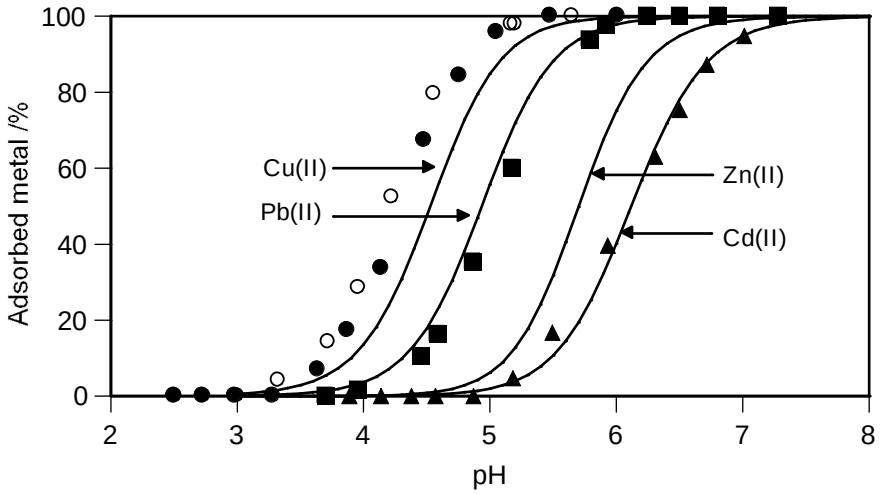

Figure 5.3 Adsorption of Cu(II) (○), Pb(II) (●), Zn(II) (■) and Cd(II) (▲) to goethite and schwertmannite as a function of pH with metal/mineral ratios of 0.057 µmol m^{-2}, a solid concentration of 1 g dm^{-3} and a specific surface area of 200 m^2 g^{-1}. The model lines for adsorption to goethite are calculated with data from Palmqvist *et al.*[100]

Figure 5.3 also show that all of the studied metals except Cd(II) have a higher affinity for schwertmannite than goethite. The higher affinity for the schwertmannite surface could potentially be explained by the formation of ternary surface complexes involving the surface hydroxyls, SO_4^{2-} and metal ions. Whether this indeed is the case can not be answered by the results described here. Therefore, an EXAFS study was conducted as described in the next section.

5.2 EXAFS

The results from the batch adsorption experiments above give a good idea about the amount of each metal that is removed from solution at a given pH. The question to answer now is, how are the metal ions removed from suspension? Do they form a precipitate, are they incorporated into the tunnel structure of schwertmannite or are they truly adsorbed to the schwertmannite surface? These questions are important to answer as a metal ion incorporated into the solid structure of a mineral is less likely to be remobilised than an ion adsorbed to a surface undergoing a pH change. With EXAFS it is possible to answer these types of questions and in addition, to answer how and to which element the metal ion coordinates. Cu(II) and Cd(II) were chosen as they are removed from solution at significantly different pH values and it could therefore be expected that the two metal ions are removed by different mechanisms. When interpreting the data in the metal-schwertmannite systems, one should bare in mind the transformation of schwertmannite to goethite, discussed in Chapter 3 and Paper 1.

5.2.1 Cu(II)-schwertmannite

In Paper 2 the adsorption of Cu(II) was studied as a function of pH, surface loading and ageing time. EXAFS spectra were collected for samples in the pH range 5-8 with two different Cu(II)/schwertmannite ratios (0.52 and 2.6 μmol m^{-2}) after 1 h and 1 month for the lower ratio and after 1 month for the higher ratio. The pH values of about 5, 6 and 8 (for exact values cf. Paper 2, Table 1) correspond to an adsorbed amount of ~60% (pH 5), ~100% (pH 6) and an amount well above the adsorption edge (pH 8). The general appearance of the Fourier transforms for all data sets is similar (Figure 5.4) with three peaks, representing three shells of atoms at distances of ~2, 3 and 4 Å (corrected for phase shift). The first shell of all samples was best fit with ca. 4 oxygen atoms at an average distance of 1.96 Å from an absorbing Cu atom, in good agreement with reports of Jahn-Teller distorted Cu(II)

complexes[101]. In order to resolve the higher shells, the obtained schwertmannite spectra were compared with results from the Cu(II)-goethite system in Paper 2. In this system two Cu-Cu distances at 2.98 and 3.3 Å are identified at pH>5.3, indicating the formation of multinuclear complexes or surface precipitates of $Cu(OH)_2$-like phases[102,103]. At pH 4.8 two Cu-Fe distances at 3.62 and 3.93 Å are suggested and tentatively attributed to a bridging bidentate complex ($(\equiv FeO)_2Cu$), analogous to the Cd(II)-goethite system[94].

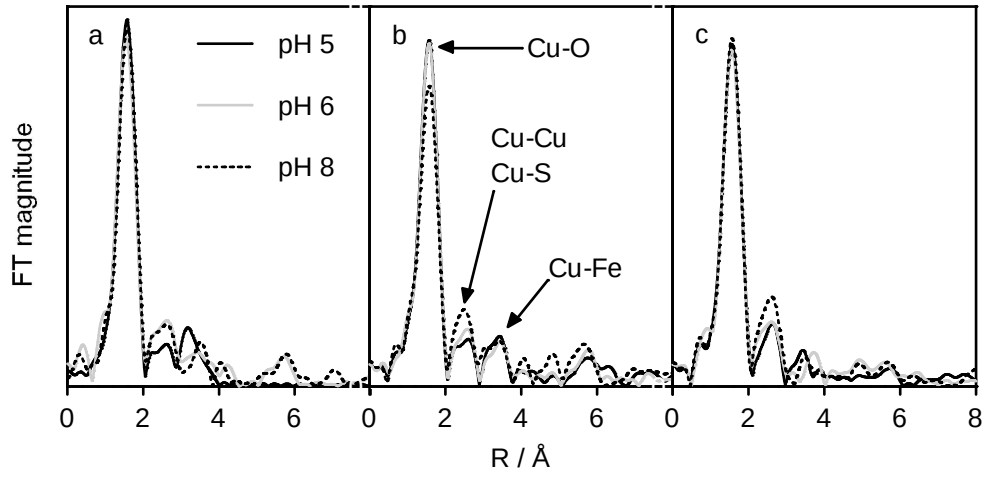

Figure 5.4 Fourier transformed EXAFS data for Cu(II) adsorbed on schwertmannite pH 5-8 a) Cu(II)/schwertmannite = 0.52 µmol m^{-2}, spectra collected 1 hour after sample preparation b) Cu(II)/schwertmannite = 0.52 µmol m^{-2} after 1 month and c) Cu(II)/schwertmannite = 2.6 µmol m^{-2} after 1 month. Distances are not corrected for phase shift.

As described in Chapter 3 and Paper 1, schwertmannite contains significant amounts of SO_4^{2-} both in the bulk structure and at the surface and this is reflected in the EXAFS results. In the Cu(II)-schwertmannite system the second shell cannot be described by Cu-Cu distances only, a Cu-S distance had to be introduced. The experimental data could satisfactorily be fit with a Cu-Cu distance at 3.0 Å and a Cu-S distance at 3.3 Å. The Cu-S distance is in agreement with a monodentate coordination between Cu(II) and SO_4^{2-}. The low coordination numbers (Paper 2, Table 1) indicate that no large aggregates form although small clusters may form as pH increases. As both distances grow in importance with pH the two distances are assumed to be associated with the same surface species.

The third shell at ~4 Å was not resolved for all samples (Paper 2, Table 1) but for six samples it could be modelled with the Cu-Fe distances derived

in the Cu(II)-goethite system though slightly shorter, 3.5 and 3.8 Å. Changes in coordination numbers in the third shell were not correlated to changes in coordination numbers in the second shell.

The results presented in Paper 2 and discussed above indicate that two Cu(II) surface species exist in the Cu(II)-schwertmannite system. One is similar to the U(VI) species suggested by Walter *et al.*[95], i.e. a ternary type B surface complex (≡Fe-SO_4-Cu). However, the increasing Cu-S and Cu-Cu coordination numbers with increasing pH suggest that the initial surface complex is converted into a precipitate-like phase. In the other surface complex, Cu(II) is directly coordinating to the surface in a bridging bidentate mode ($(\equiv FeO)_2Cu$). The ageing of the samples implies that schwertmannite is partly transformed to goethite and that the surface species form at a goethite surface instead of at a schwertmannite surface. However, the same surface species form after one hour when little, if any, transformation occurs. This suggests that either the same surface species form in the Cu(II)-SO_4^{2-}-goethite system or the formation of Cu(II) surface complexes stabilises schwertmannite in the same way as suggested for AsO_4^{3-} [99] and little transformation occurs. This issue cannot be resolved with the results presented here.

5.2.2 Cd(II)-schwertmannite

The adsorption of Cd(II) as a function of pH and surface loading was also studied in Paper 2. EXAFS spectra were collected for samples in the pH range 6.6-10 with two different Cd(II)/schwertmannite ratios (0.52 and 2.6 μmol m^{-2}) after 1 month. The pH values of about 7, 8 and 10 (for exact values cf. Paper 2, Table 2) correspond to an adsorbed amount of ~60% (pH 7), ~100% (pH 8) and an amount well above the adsorption edge (pH 10). The general appearance of the Fourier transforms for all data sets is again similar (Figure 5.5) with three peaks, representing three shells of atoms at distances of ~2, 3 and 4 Å (corrected for phase shift). Due to large structural disorder of the Cd-O distance, the first shell of all samples was best fit with 3+3 oxygen atoms at 2.2 and 2.3 Å from an absorbing Cd atom.

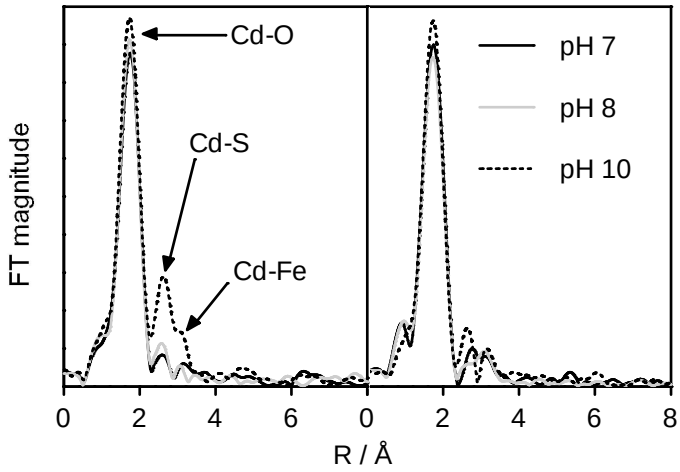

Figure 5.5 Fourier transformed EXAFS data for Cd(II) adsorbed on schwertmannite pH 7-10 a) Cd(II)/schwertmannite = 0.52 µmol m^{-2} b) Cu(II)/schwertmannite = 2.6 µmol m^{-2}. Spectra collected after 1 month. Distances are not corrected for phase shift.

In the Cd(II)-schwertmannite system the second shell could be described by two Cd-S distances at 3.3 and 3.5 Å. As both distances grow in importance with pH the two distances are assumed to be associated with the same surface species. The relatively low coordination number at pH 7 indicates a bridging bidentate coordination to surface SO_4^{2-} as suggested for U(VI)[95], i.e. a $(\equiv Fe\text{-}SO_4)_2$-Cd complex is formed. However, it should be noted that the pH is fairly high for SO_4^{2-} to be adsorbed at the surface[77] though the formation of the suggested complex might favour the adsorption. An increase in pH is accompanied by an increase in coordination number. This suggests the formation of a precipitate-like phase in agreement with the Cu(II)-schwertmannite system.

The third shell was fitted with a Cd-Fe distance of 3.8 Å, in good agreement with a bridging bidentate complex[94], i.e. a $(\equiv FeO)_2Cd$ complex. As in the Cu(II)-schwertmannite system, changes in coordination number in this shell were not correlated to changes in coordination numbers in the second shell.

The results from the Cd(II)-schwertmannite system are similar to the results obtained in the Cu(II)-schwertmannite system. Two different surface species are suggested for both systems and precipitate-like phases form as pH increases. In the Cd(II) system the question whether adsorption occurs to a goethite or a schwertmannite surface is even more relevant as the

transformation to goethite accelerates as pH increases (Chapter 3 and Paper 1). This issue calls for further studies.

5.3 Active surface sites

When discussing the potential of schwertmannite as a metal scavenger in natural attenuation processes it is not only important to investigate the pH dependency of the sorption processes but also the quantity of metal that can be adsorbed before the surface is saturated. Bigham *et al.*[45] suggested that if the proposed formula for schwertmannite was correct, the SO_4^{2-} content exceeding the S/Fe ratio of 1/8 should be adsorbed at the surface and calculated a maximum adsorption capacity of 2.6 μmol SO_4^{2-} m^{-2}, based on an akaganéite-type structure and bidentate bridging complexes to singly coordinated surface hydroxyl groups. With the Kristineberg schwertmannite this corresponds to an adsorbed amount of 540 μmol SO_4^{2-} g^{-1} (33%), equivalent to 2.65 μmol SO_4^{2-} m^{-2}. If the assumption of a bidentate complex is correct the site density is 3.19 sites nm^{-2} whereas if a monodentate surface complex is formed the site density is 1.60 sites nm^{-2}. Both values are close to those reported for akaganéite, 1.62 sites nm^{-2} by Parida *et al.*[104] and 3.33 sites nm^{-2} by Kanungo[105]. Based on the finding that two OH^- are consumed for each SO_4^{2-} released from schwertmannite, it would be easy to draw the conclusion that a bidentate complex is a valid assumption for both SO_4^{2-} in the bulk structure and at the surface. However, IR data (Figure 3.11) clearly show that the situation is more complicated, with at least two surface species of SO_4^{2-}. The same 2:1 relationship of OH^- and SO_4^{2-} could also be explained by the replacement of one monodentate SO_4^{2-} by one OH^- accompanied by a simultaneous deprotonation of a surface hydroxyl group by another aqueous OH^-.

pH-stat experiments at pH 7.5 with Cd(II) (Figure 5.6) resulted in a concentration of active surface sites of 550 μmol g^{-1}, corresponding to 2.72 μmol m^{-2}. It is possible that even more Cd(II) could be adsorbed at slightly higher pH so the site density suggested here is probably best described as being at least 2.72 μmol m^{-2}. The formation of a surface precipitate also has to be considered but EXAFS data in Paper 2 suggest that this is of minor importance at the studied pH. If Cd(II) form bidentate complexes at the surface, as suggested from the EXAFS data above, the site density is 3.28 sites nm^{-2}.

The site density used by Swedlund and Webster[92] for their modelling of Cu(II) and Zn(II) adsorption to schwertmannite is that of ferryhydrite from Dzombak and Morel[106], i.e. 0.005 mol mol^{-1} Fe(III) of high affinity sites and 0.200 mol mol^{-1} Fe(III) of low affinity sites. According to the

discussion and results presented above, this is probably an overestimation of the available sites. 2.72 μmol sites m^{-2} corresponds to 0.125 mol sites mol^{-1} Fe(III), assuming bidentate bonding. Ferrihydrite particles are smaller in size, 4-6 nm in diameter[44] compared with ~400 nm of schwertmannite (Chapter 3 and Paper 1) which explains that a larger portion of Fe-atoms are present as surface groups in ferrihydrite.

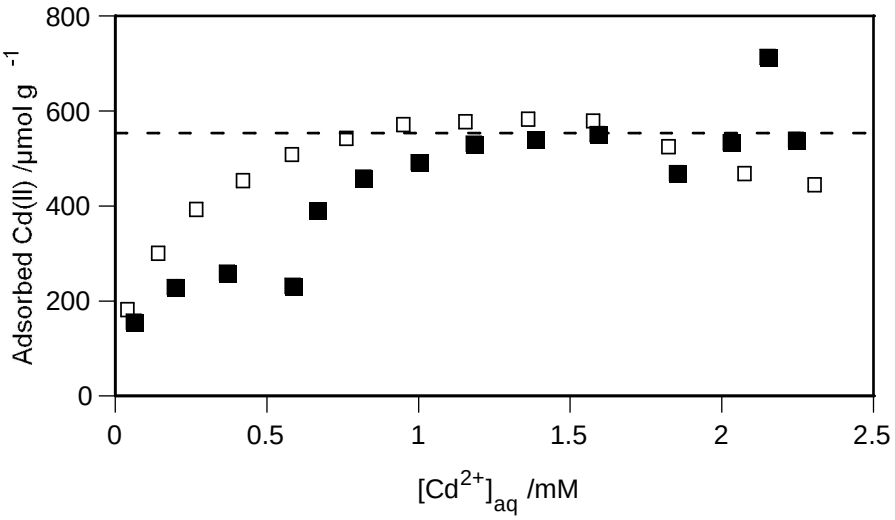

Figure 5.6 Adsorption isotherm of Cd(II) to schwertmannite at pH 7.5 with an initial solid concentration of 1 g dm^{-3}. The different symbols represent different experiments performed under the same conditions. The average maximum adsorption capacity of 550 μmol g^{-1} is indicated by a dotted line.

pH-stat experiments with Cd(II) at pH 8.5 and Zn(II) at pH 7.5 did not yield the plateau observed in Figure 5.6. This can be related to precipitation in some cases where a maximum in aqueous concentration were reached. However, in some cases neither a plateau nor a maximum aqueous concentration was reached. In these cases, the suspension was left standing with stirring for three days after the last addition of metal ion. When sampling again after the three days the aqueous metal concentration had decreased. This might indicate that precipitation was kinetically controlled[15].

From the perspective of natural attenuation it is interesting to know how the adsorption capacity relates to the aqueous concentration of heavy metals in AMD, i.e. are there enough surface sites to adsorb all of the aqueous heavy metals in the AMD? A simple calculation can give the answer to this question. Assuming the AMD characterised in Paper 5 represents a typical

AMD in Kristineberg and that all Fe(III) forms schwertmannite with the composition given in Section 3.2 ($Fe_8O_8(OH)_{5.02}(SO_4)_{1.49}$), a suspension of 3.4 g dm^{-3} forms. With a surface area of 200 m^2 g^{-1} and a surface site "concentration" of 2.7 μmol m^{-2}, the total concentration of surface sites in 1 dm^{-3} suspension is about 1.8 mM. The concentrations of Ca^{2+} and Mg^{2+} are very high (10.9 and 8.3 mM, respectively) and these can not be expected to decrease in any significant amount due to adsorption to schwertmannite. These ions also adsorb weakly and are of minor importance in the context of toxicity. Neglecting SO_4^{2-}, Ca^{2+} and Mg^{2+} gives an ion concentration of 1.5 mM, corresponding to 80% of available surface sites. The list of ions that probably adsorb can be shortened even further as Na^+ and K^+ do not adsorb to any significant extent and Mn^{2+} and Al^{3+} would probably form precipitates (Section 1.2). The concentration of ions likely to adsorb is then reduced to 0.4 mM, 20% of the concentration of surface sites, i.e. the potential of reducing heavy metal by adsorption processes is large. Similar calculations can be made for the tailings, assuming total dissolution and subsequent precipitation of schwertmannite. These calculations lead to the same conclusion; there are more surface sites than heavy metals and toxic anions and natural attenuation by sorption processes could thus be very useful in reducing the concentration of these contaminants. However, one important criterion is that the acididity of the AMD is controlled or the adsorption potential will not be fully utilised due to low pH.

5.4 Partitioning coefficients

The goal for the studies above is to describe the adsorption of heavy metals to schwertmannite in terms of surface complexation and to calculate equilibrium constants. This is complicated by a number of factors, e.g. the transformation to goethite, the release of SO_4^{2-}, and the existence of multiple surface complexes involving both metal ions and SO_4^{2-} and is yet to be done. An alternative description of adsorption in terms of surface complexation is to derive partitioning coefficients, K_d, which are defined as:

$$K_d = C_S\, C_L^{-1} \qquad (5.1)$$

where C_S is the amount associated with the solid (mol g^{-1}) and C_L is the concentration in solution (mol dm^{-3}). K_d is widely used in geochemical modelling to quantify retention by solid phases. Unfortunately, K_d is conditional and the value determined is only valid at the specific conditions under which it was determined. Adsorption of metal ions to mineral surfaces is very pH dependent and a range of K_d values have therefore been calculated and tabulated in Table 5.1. For Cu(II), Pb(II) and Cd(II) the

values have been estimated from data upon which the adsorption isotherms in Figure 5.1a and 5.1b are based. As the adsorption isotherms for Cu(II) and Pb(II) are very similar, the K_d values are set to be identical for the two metals. For Zn(II) the agreement between data sets was not as good as for the other metal ions. The K_d values have therefore been separated in Table 5.1 where values for "Zn(II) low" are estimated from the data of Figure 5.1a and "Zn(II) high" from the data of Figures 5.1b and 5.1c. The reason for blank fields in Table 5.1 is that K_d cannot be estimated in the pH ranges where the metal ions are adsorbed to 0 or 100%.

Table 5.1 log K_d for metal partitioning by schwertmannite.

pH	Cu(II)	Pb(II)	Cd(II)	Zn(II) low	Zn(II) high
3.5	-1.04	-1.04			
4.0	-0.34	-0.34		-1.71	
4.5	0.42	0.42		-0.85	-1.12
5.0	1.06	1.06	-1.79	-0.01	-0.63
5.5	2.14	2.14	-0.79	0.61	-0.24
6.0			-0.20	2.05	0.14
6.5			0.38		0.74
7.0			1.11		1.52
7.5			1.28		
8.0			2.00		

6 NOM ADSORPTION

In nature NOM is found everywhere and is well known to adsorb to mineral surfaces. The amount adsorbed is dependent on pH and NOM concentration but also on the mineral. As NOM is negatively charged, due to deprotonated functional groups, the adsorption to acidic minerals such as silica is small, since these minerals have a negative surface charge even at relatively low pH. The adsorption to Fe(III) oxides is far more favourable as these minerals have a positive surface charge even at relatively high pH[107,108]. The adsorption of NOM to the surface of Fe oxides can have a significant influence on the surface properties. Adsorption of negatively charged NOM to a positively charged surface may cause a charge reversal of the particle even at low coatings of NOM[109]. This can potentially have a large effect on metal adsorption as negatively charged particles are more likely to attract cations.

6.1 NOM-goethite

The adsorption of NOM to goethite was investigated for the two NOM samples collected from Svartbergets Forest Research Area in 1998 and 1999 and described in Chapter 4. The results for the NOM-goethite systems are presented in Figure 6.1 (1998 sample) and 6.2 (1999 sample, Paper 3).

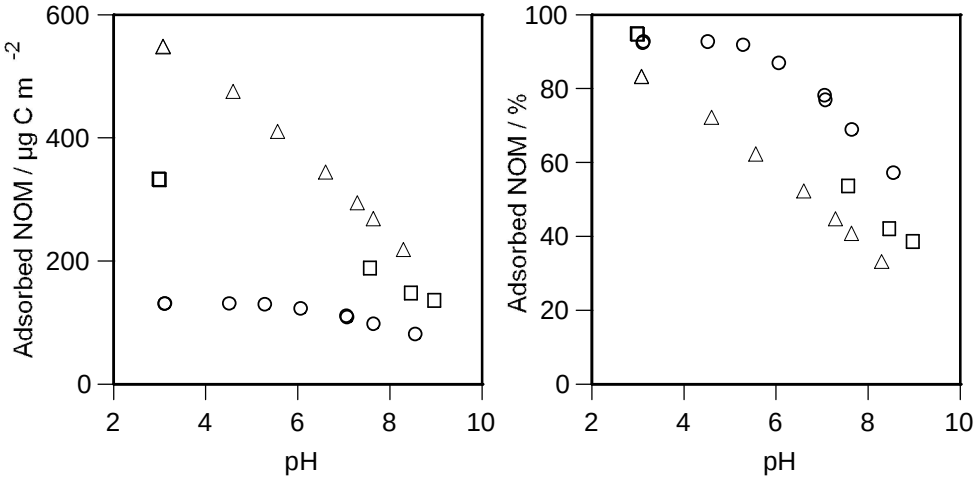

Figure 6.1 Adsorption of NOM (1998 sample) to goethite at NOM/goethite ratios of 140 (○), 350 (□) and 660 (Δ) µg C m^{-2}. Initial goethite (NOM) concentration of 4.6 (26), 3.0 (42) and 2.7 (70) g dm^{-3} (mg C dm^{-3}), respectively, with a specific surface area of 39.9 m^2 g^{-1} for the goethite.

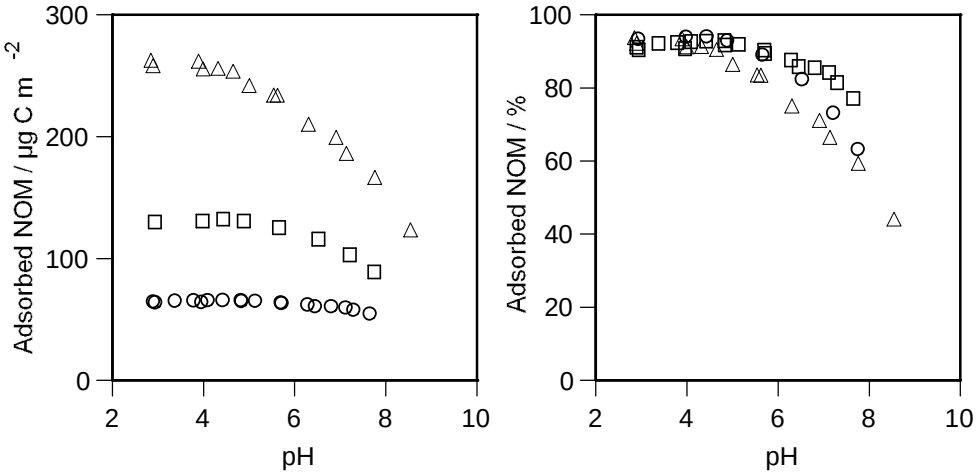

Figure 6.2 Adsorption of NOM (1999 sample) to goethite at NOM/goethite ratios of 70 (○), 140 (□) and 280 (Δ) µg C m^{-2}. Initial goethite (NOM) concentration of 4.9 (14), 3.3 (19) and 2.3 (27) g dm^{-3} (mg C dm^{-3}), respectively, with a specific surface area of 42.1 m^2 g^{-1} for the goethite. The highest and lowest ratios include both adsorption and desorption data.

The results might appear slightly different for the two samples but this is due to the different NOM/goethite ratios used. A comparison between the two samples (Figure 6.3) shows that the adsorption is very similar.

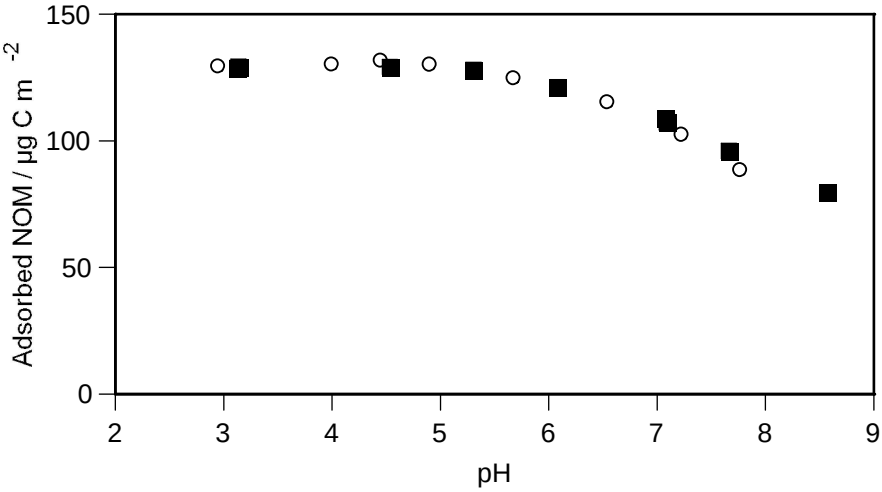

Figure 6.3 Adsorption of NOM to goethite with a NOM/goethite ratio of 140 µg C m^{-2} for the 1998 (■) and 1999 (○) sample.

The adsorption of the two NOM samples shows typical anionic behaviour that is well known for humic substances, i.e. adsorption decreases as pH increases[107,110-112]. pH-stat experiments at pH 4 and 5 with the 1998

sample and goethite (Figure 6.4) confirm that adsorption at low NOM concentrations is similar at the two different pH values. This is to be expected, considering the adsorption isotherms for the low NOM/goethite ratio in Figure 6.1 and 6.2. As the NOM concentration increases however, the adsorption is higher at pH 4 than at pH 5 and this in accordance with results for the higher NOM/goethite ratios in Figure 6.1 and 6.2. This behaviour can be explained by considering the charges of both NOM and the goethite surface. Goethite has a pH_{iep} = 9.4[59], i.e. at lower pH the surface is positively charged due to protonation of the surface hydroxyl groups. NOM on the other hand has carboxylic groups that are deprotonated, more so at pH 5 than pH 4. As NOM adsorbs to the goethite, the more negative charge of the NOM at pH 5 causes larger electrostatic repulsions between the different NOM "molecules", thus the lesser adsorption at the higher pH. The increased charge of the NOM "molecule" will also cause internal repulsion, resulting in a flatter three-dimensional configuration at the surface[113]. As each NOM "molecule" occupies a larger area, this will also decrease the adsorption as pH increases. The decrease in positive charge of the surface as pH increases also decreases the adsorption.

Besides the electrostatic interactions, hydrophobic interactions and specific adsorption are also likely to occur as NOM adsorbs at $pH>pH_{iep}$, i.e. where the surface is negatively charged[111,114,115]. The hydrophobic interactions might occur since NOM possibly contains parts that are lacking functional groups, i.e. hydrocarbon branches, that have a higher affinity for the surface than the solution. The specific adsorption could be ascribed to direct interaction (inner sphere complexation) between e.g. carboxylic groups and the surface hydroxyl groups and also to hydrogen bonding[110].

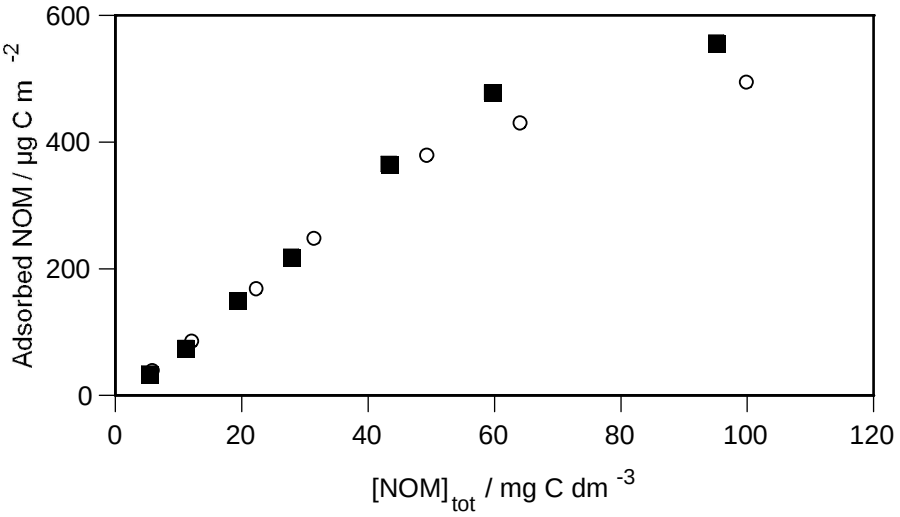

Figure 6.4 Adsorption isotherms at pH 4 (■) and pH 5 (○) for the 1998 NOM sample on goethite. Initial goethite concentration of 4.0 and 3.8 g dm^{-3}, respectively with a specific surface area of 32.5 m^2 g^{-1}.

6.2 NOM-schwertmannite

The adsorption of NOM to schwertmannite was investigated for the 1999 sample only. The results for the NOM-schwertmannite systems are compared with the NOM-goethite system in Figure 6.5.

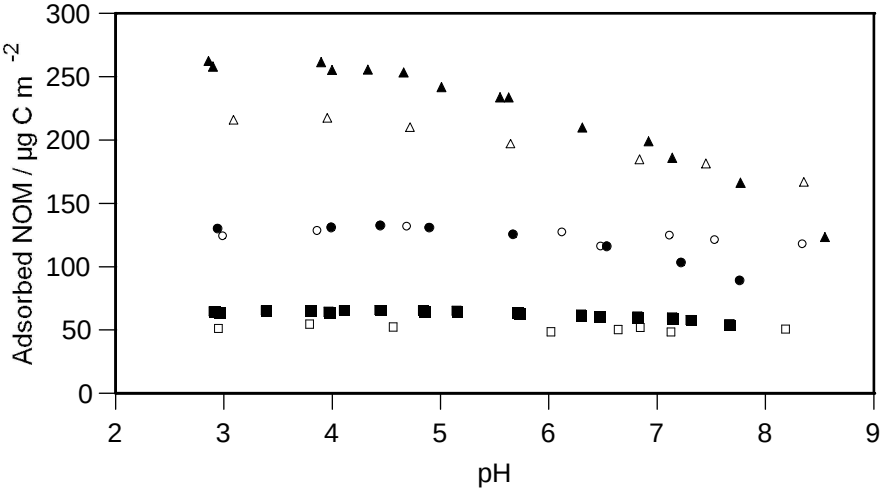

Figure 6.5 Adsorbed amount of NOM to goethite (filled symbols from Figure 6.2) and schwertmannite (open symbols) as a function of pH. The symbols represent NOM/mineral ratios of: 70[58] (■,□), 140[145] (●,○) and 280[290] (▲,Δ) µg C m^{-2} with schwertmannite ratios in square brackets.

For the two lowest NOM/mineral ratios the differences between the two minerals are quite small at low pH but slightly less NOM is adsorbed to the schwertmannite surface on a percent basis. At the highest ratio, considerably less NOM is adsorbed to the schwertmannite surface compared to goethite. This is likely to be an effect of adsorbed SO_4^{2-}, as an increasing concentration of SO_4^{2-} causes NOM to desorb from the goethite surface, Figure 6.6. At a SO_4^{2-} concentration of 2 mM, about 10% less NOM is adsorbed compared to in the absence of SO_4^{2-}. This has also been shown for NOM adsorption to hematite[111].

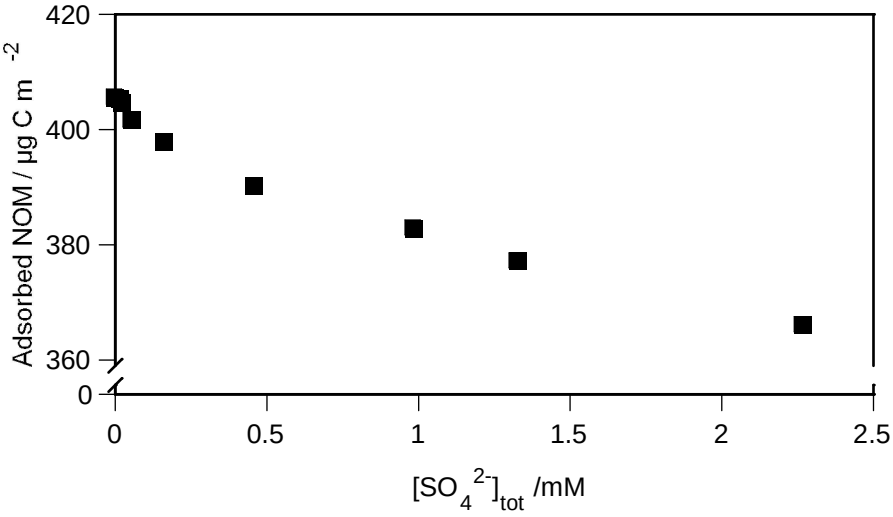

Figure 6.6 Influence of SO_4^{2-} on NOM adsorption for the 1998 NOM sample at pH 3.5. NOM/goethite ratio = 440 µg C m^{-2}. Initial goethite (NOM) concentration of 3.3 (47) g dm^{-3} (mg C dm^{-3}) with a specific surface area of 32.5 m^2 g^{-1} for the goethite.

At high pH the adsorption of NOM to schwertmannite is greater than to goethite at all ratios. This could be attributed to SO_4^{2-} adsorbed at the surface of schwertmannite at low pH, competing with NOM for the available surface sites. The adsorbed SO_4^{2-} also decreases the positive surface charge and thus makes the surface less attractive for NOM. As pH increases, SO_4^{2-} is released from the surface (Section 3.4) and this favours NOM adsorption. The XPS study described in Paper 1 also showed that the schwertmannite sample contains carbon at the surface. This additional carbon can compete with the added NOM, resulting in an apparently lower NOM adsorption.

The fact that more NOM is adsorbed to schwertmannite than to goethite at high pH is somewhat puzzling. The surface of schwertmannite develops a

negative charge at a lower pH than goethite (pH 7.2 and 9.4, respectively) and this would suggest more adsorption to goethite unless the specific adsorption of NOM is stronger to the schwertmannite surface. The higher adsorption could possibly be due to the presence of trace metals in the schwertmannite sample (Section 3.2) as these can enhance NOM adsorption at high pH as will be discussed in the next chapter.

7 NOM-Cu(II)-MINERAL

In the two previous chapters the adsorption of metals and NOM to mineral surfaces has been studied. These systems are of course interesting by themselves but in order to fully understand processes in nature, where NOM, Cu(II) and minerals are mixed, this combination should be investigated. The interesting questions to answer concern whether NOM and Cu(II) interact when adsorbing to a mineral surface and if so, how does the interactions affect the adsorption. In this chapter NOM-Cu(II)-mineral systems are studied, where the minerals are goethite and schwertmannite.

7.1 NOM-Cu(II)-goethite

The mutual influence of NOM (1999 sample) and Cu(II) on adsorption to goethite was investigated for three NOM/goethite ratios in the pH range 3-9 keeping the Cu(II)/goethite ratio constant. There is a clear difference between Cu(II) adsorption in the Cu(II)-goethite and NOM-Cu(II)-goethite systems (Figure 7.1). As the NOM-concentration increases, the adsorption edge for Cu(II) is shifted towards lower pH. This is a well known effect and can be explained by considering that negatively charged NOM adsorbs to the mineral surface and lowers the positive charge at the surface and thereby favours the binding of positively charged Cu(II) ions to the surface[116]. Increased metal uptake in presence of complexing ligands may also be explained by the formation of ternary surface complexes involving metal ions, ligands and surface functional groups[117,118]. Alcacio *et al.*[119] studied the adsorption of Cu(II) to goethite in the presence of humic acids at pH 5.6 with EXAFS and suggested that ternary surface complexes of type A (≡Fe-Cu(II)-HA) were dominating at low concentrations of HA but as the concentration increases, HA replaces Cu(II) at the surface and type B complexes (≡Fe-HA-Cu(II)) form. Vermeer *et al.*[120] suggests that the increased Cd(II) adsorption to hematite in the presence of HA is due to a decrease in surface potential when HA adsorbs, corresponding to an increase in pH of one pH unit.

As pH increases and NOM desorbs, Cu(II) could be mobilised if associated with NOM[116]. This could possibly be the case for the lowest concentration of NOM between pH 4-6 in Figure 7.1a where the experimental points are slightly lower compared to the model for Cu(II)-goethite from Palmqvist *et al.*[100]. It is also well documented that Cu(II) and other metal ions form complexes with NOM in solution[82,86,121,122]. Using equilibrium constants from Lövgren and Sjöberg[121] it can be shown that, in the absence of goethite, a Cu(II)-NOM complex forms in solution in the pH

range 4-6.5 for the concentrations used in the experiment. A maximum of about 9% of the total amount of Cu(II) forms a complex at pH 5.6.

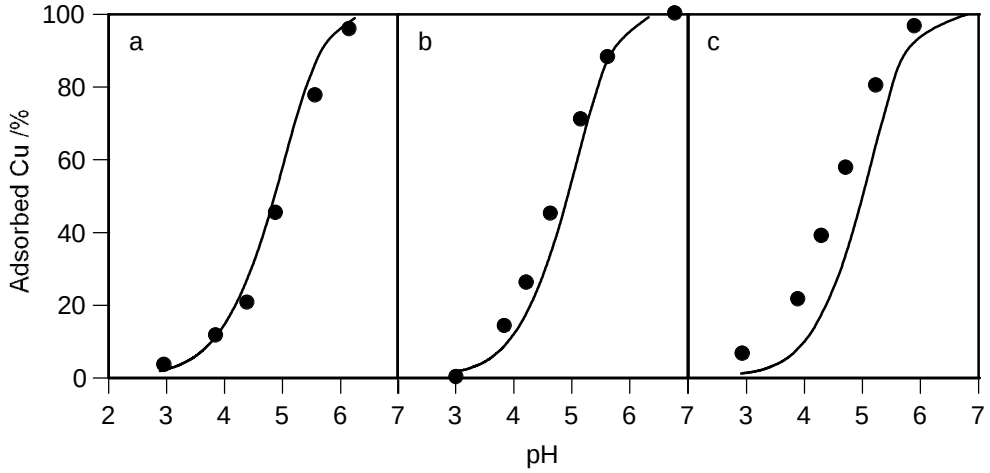

Figure 7.1 The effect of NOM on Cu(II) adsorption to goethite as a function of pH. The symbols represent NOM/goethite ratios of a) 67, b) 134, and c) 268 μg C m^{-2}, corresponding to $[Cu(II)]_{tot}/[H_2A]_{tot}$ ratios of 8.1, 3.9 and 2.0, respectively. The solid line represents the absence of NOM, calculated with formation constants from Palmqvist *et al.*[100]. $[Cu(II)]_{tot}$ = 1.79-1.87 μmol m^{-2}.

The addition of Cu(II) to the NOM-goethite system had a noticeable influence on NOM adsorption as can be seen in Figure 7.2. For the lowest NOM/goethite ratio (67 μg C m^{-2}) and at low pH, the percentage of adsorbed NOM is lower in the presence of Cu(II) than in the NOM-goethite system. The adsorption reaches a local minimum around pH 5 where only 75% is adsorbed compared to 92% in the absence of Cu(II). This can possibly be due to formation of a soluble Cu(II)-NOM complex as the pH-values for the decrease in NOM adsorption coincide with the slight shift in Cu(II) adsorption for this ratio in Figure 7.1. Using equilibrium constants from Lövgren and Sjöberg[121] it can also be shown that, in the absence of goethite, >70% of the NOM forms a Cu(II)-NOM complex at pH 5.6 with the concentrations given in Figure 7.2a. One might then speculate that the type A complex suggested by Alcacio *et al.*[119] could be a combination of Cu(II) adsorbed directly to the surface and a type B ternary surface complex as results obtained with EXAFS analysis represent the average scattering effect.

As pH then increases more NOM is adsorbed and for the highest pH the amount of NOM adsorbed is larger with Cu(II) present than without. The increased adsorption at high pH is most pronounced for the highest ratio where an additional 23% NOM is adsorbed around pH 8. The increased

adsorption at high pH can be explained by the formation of a type A ternary surface complex, as Cu(II) adsorbs at the goethite surface and NOM binds to the adsorbed Cu(II). The adsorption of Cu(II) will also makes the surface more positively charged, which also attracts the negatively charged NOM.

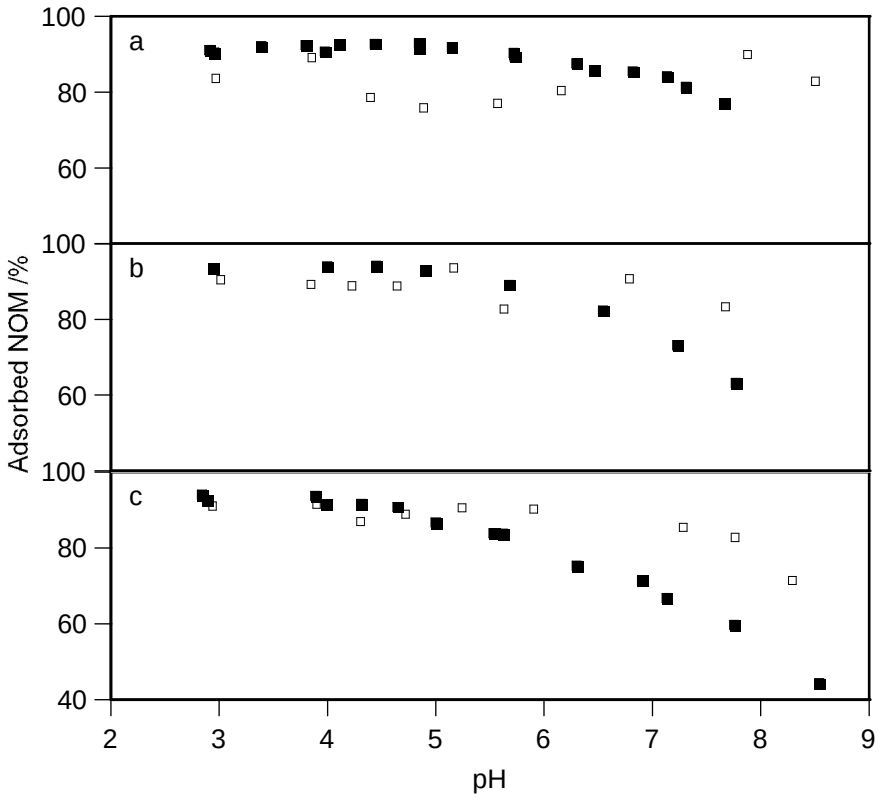

Figure 7.2 The effect of Cu(II) on NOM adsorption to goethite as a function of pH. The symbols represent absence of Cu(II) (■) and Cu(II) present (□) at the NOM/goethite ratios of a) 70 [67], b) 140 [134], and c) 280 [268] μg C m^{-2}. The ratios when Cu(II) is present are in square brackets. $[Cu(II)]_{tot}$ = 1.79-1.87 μmol m^{-2}.

7.2 NOM-Cu(II)-schwertmannite

In contrast to the above described NOM-Cu(II)-goethite system, no major effects were observed in the NOM-Cu(II)-schwertmannite system, Figure 7.3. The quantification of NOM adsorption in Figure 7.3 is based on UV measurements and these turned out to be rather unreliable in the presence of schwertmannite and differed markedly from the DOC measurements. Samples with schwertmannite only had a significant, and in relation to pH, scattered absorption at 260 nm making a background subtraction difficult,

especially at low NOM concentrations. This is probably a combined effect of release of both SO_4^{2-} and organic carbon from schwertmannite. The results presented for NOM adsorption in Figure 7.3a should therefore be interpreted with caution. DOC measurements also showed an influence from schwertmannite but were more reliable and could be handled with background subtraction.

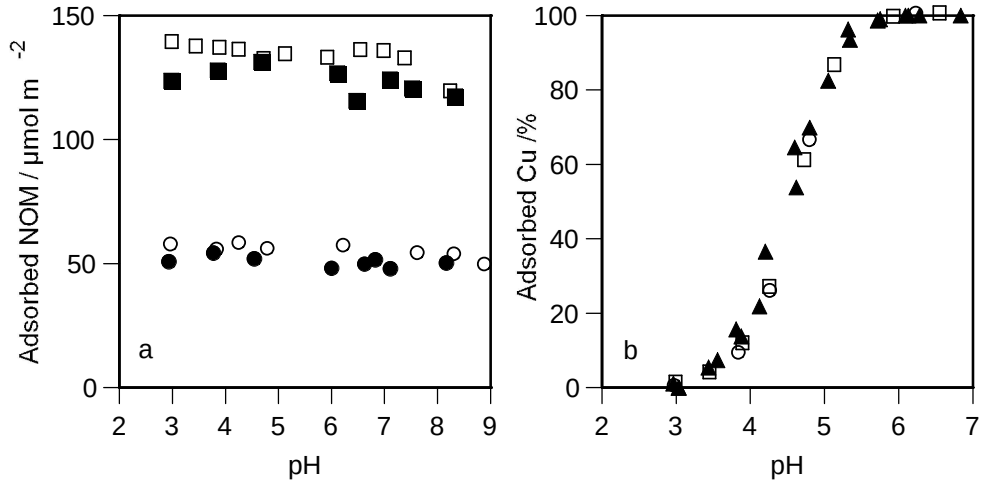

Figure 7.3 The adsorption of NOM (a) and Cu(II) (b) to schwertmannite as a function of pH in the NOM-Cu(II)-schwertmannite system. In the left figure the filled symbols represent absence of Cu(II) (●,■) and open symbols represent [Cu(II)] = 0.52 µmol m^{-2} (○,□) at the NOM/schwertmannite ratios of 58 (●,○) and 145 (■,□) µg C m^{-2}. In the right figure the symbols represent no NOM present (▲) and 58 (○) and 145 (□) µg C m^{-2}.

8 OTHER SECONDARY IRON PRECIPITATES

The previous chapters have concentrated on the minerals schwertmannite and goethite, of which the former was found at the Kristineberg mine and the latter is the end-product of schwertmannite transformation in suspension. As discussed in Section 1.2, these are not the only two minerals that may be formed from AMD and the phases formed depend strongly on pH. At the Kristineberg mine the effluent water from the tailings impoundment is currently treated with lime to increase pH and precipitate metal hydroxides. The possibility of re-directing a small creek to dilute the AMD in a water-covered impoundment has also been discussed. A study was therefore undertaken (Paper 5) to determine the Fe(III) phases expected to precipitate if the pH of AMD from Kristineberg was increased with either base or a combination of base and surface water rich in organic carbon (NOM 1999 sample). The study was conducted as pH-stat experiments at pH 5.5 and 7 as described in Paper 5. The formation of precipitates was studied at both 10°C and 25°C. As 10°C is a more relevant temperature for the conditions in Kristineberg, only these results are discussed here though basically the same results were obtained at 25°C. As the same results are obtained at both temperatures, the conclusions from Paper 5 should apply to a rather wide temperature range.

8.1 Chemical composition of AMD

The AMD sample was collected in 2001 at the inlet to a permeable reactive barrier system, installed in the summer of 1999[5]. The samples were immediately acidified to ~pH 1 with $HClO_4$ to prevent oxidation of Fe(II). pH was 4.1 before acidification. The elemental composition is given in Table 8.1. As a comparison, the concentration of Fe corresponds to a suspension of 3 g dm^{-3} assuming all of the Fe forms goethite. This is close to the goethite concentrations used in Chapter 6 and 7.

Table 8.1 Elemental composition of the unfiltered AMD sample. Concentrations in μM, except Hg which is in nM.

S 52 100	K 410	Mn 160	Co 0.45	As 0.04	Mo <0.01
Fe 34 200	Si 390	Zn 28	Ba 0.13	Pb 0.02	Hg 0.02
Ca 10 900	Na 330	Sr 5.9	Cu 0.12	Cd 0.004	
Mg 8 300	Al 220	Ni 0.90	Cr 0.08	P <10	

8.2 Mineralogy and surface area of precipitates

All of the precipitates formed were dark red-brown in colour. At pH 7 lepidocrocite (γ-FeOOH) could easily be identified by the XRD pattern (Figure 8.1) in both the absence and presence of NOM.

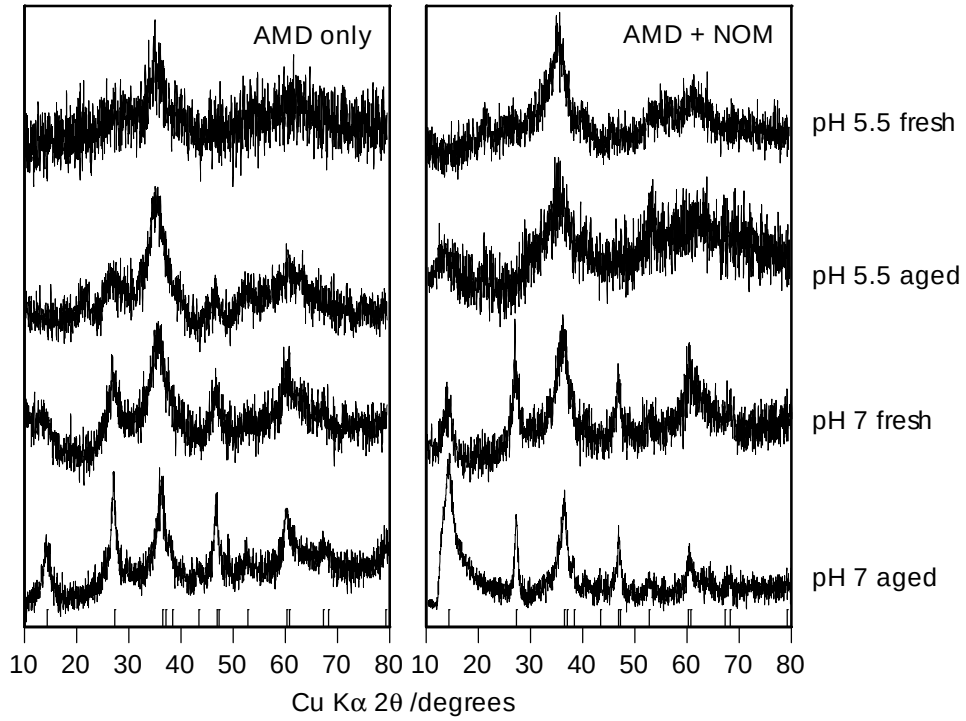

Figure 8.1 XRD pattern of precipitates formed from Kristineberg AMD at different pH values and NOM concentrations. The lines in the bottom of the figures represent lepidocrocite (PDF 44-1415).

The main difference between absence and presence of NOM is the surface area of the precipitates, Table 8.2. In the absence of NOM the fresh precipitate has a high surface area that is halved after 24 days ageing, indicating a growth of the precipitated particles. When NOM is present the surface area is lower for the fresh precipitate but does not change much during ageing. If the adsorption of NOM to lepidocrocite is similar to adsorption to schwertmannite and goethite, described in Chapter 6, a substantial amount of NOM is adsorbed at the lepidocrocite surface. The adsorbed NOM could potentially cause aggregation of the particles and thereby lower the surface area of the fresh precipitate compared to when no NOM is present. Adsorbed ions are also known to reduce crystal growth[44] and this is a likely explanation for the rather constant surface area in the presence of NOM.

Table 8.2 Specific surface area (SSA), in m^2 g^{-1}, of the different AMD precipitates formed at 10°C and the aqueous Zn concentration in µM.

Sample	Fresh		Aged 17-24 days		Aged 34 days	
	SSA	$[Zn^{2+}]$	SSA	$[Zn^{2+}]$	SSA	$[Zn^{2+}]$
pH 5.5	116	4.1	136	0.3		
pH 5.5 + NOM	150	2.3	97	2.3		
pH 7	207	0.3	105	0.3		
pH 7 + NOM	167	0.1	154	0.1		
pH 8 + Zn	27	10.6	64	1.3	84	0.8

At pH 5.5 the situation is more complex. For the fresh precipitate with AMD only, 2-line ferrihydrite is probably the phase formed with peaks at about 2.54 and 1.51 Å in the XRD pattern (Figure 8.1). After ageing and in the presence of NOM additional peaks emerge. No single phase can explain the observed patterns. Bigham *et al.*[14] found a mixture of ferrihydrite and schwertmannite at this pH and it is probably a similar mixture that has precipitated in the current study, together with traces of goethite and lepidocrocite. No clear trends can be observed regarding the surface area of the solid phases formed at pH 5.5.

8.3 Natural attenuation of Zn

The attenuation of the ambient Zn concentration was monitored for the samples described above (Table 8.2). For all of the samples at pH 7 and for the pure AMD samples at pH 5.5, the reduction in the amount of aqueous Zn was >98%. The reduction is either due to adsorption of Zn to the surface of the Fe precipitates, co-precipitation with Fe or a combination of the two processes. When NOM was present at pH 5.5 the reduction in the amount of aqueous Zn was only 80%, which indicates that soluble Zn-NOM complexes form.

The removal of Zn from solution was further studied by addition of extra Zn(II) (Fe/Zn = 10) to the AMD and studied at pH 8. It was not possible to identify the phases formed but XPS analysis indicated that the fresh precipitate was a coprecipitate of Fe(III) and Zn(II) with Zn(II) possibly adsorbed to the surface as well. Curiously enough the surface area increased significantly during ageing (Table 8.2), possibly due to structural rearrangements as the XRD patterns also changed with ageing (Paper 5, Figure 6) The aqueous Zn(II) concentration was immediately reduced by >99% and decreased steadily (Table 8.2). The decrease with ageing is possibly an effect of the rearrangements leading to more available surface sites, that the kinetics of adsorption are slow or that the affinity for Zn(II) is different for the different phases formed during ageing.

CONCLUDING REMARKS

In this thesis a number of techniques have been utilised in an attempt to answer some of the questions regarding the potential of Fe(III) precipitates as metal scavengers in AMD. In the MiMi programme the field site common for the programme is the Kristineberg mine and all of the research within this programme has the conditions at Kristineberg as the "base case", i.e. What implications do our findings have for the Kristineberg mine site? It is then intended to implement the knowledge gathered for this site in future measures to mitigate the impact of mining waste, not only at the Kristineberg mine but for the mining industry at large.

This thesis shows that schwertmannite might be the dominating secondary precipitate forming at Kristineberg and at the low pH and low temperature prevailing in Kristineberg (annual mean temperature ~1°C)[3] schwertmannite is stable, though some transformation to goethite may occur during summer. Schwertmannite is an acidic mineral and the acidity produced during transformation to goethite can be calculated from the SO_4^{2-} content. SO_4^{2-} is partly adsorbed to the schwertmannite surface and forms two different surface complexes that are similar to the complexes formed at the goethite surface. Of the metal ions investigated, only Cu(II) and Pb(II) can be expected to adsorb in any significant amount to schwertmannite in the environment where schwertmannite is likely to be the dominating phase precipitating (pH 2.8-4.5). Zn(II) and Cd(II) do adsorb to schwertmannite but at pH values where schwertmannite might at most be a minor constituent of the secondary precipitates formed. If natural attenuation of a wide range of heavy metals is to be achieved, pH has to be raised to a value where the desired metal ions are removed by adsorption and/or precipitation processes. This might also have implications on the stability of the schwertmannite present and consequently on the amount of lime needed to both raise pH and to neutralise the acidity from transformation of schwertmannite to goethite.

The acid-base properties of Kristineberg NOM could probably be estimated with any of the three models described in Paper 4. However, the concentration of metal ions is very high and the formation of soluble metal-NOM complexes has to be taken into consideration. The high concentrations of Fe(II) and Fe(III) in particular need consideration. WHAM V takes into account the formation of Fe(III)-NOM complexes and the calibrated version described in Paper 4 might then be a good choice.

NOM adsorbs to the surfaces of schwertmannite and goethite in similar amounts and SO_4^{2-} can, by competition for surface sites, decrease the

amount of NOM adsorbed. This could potentially increase the amount of aqueous metal-NOM complexes and thus increase the aqueous concentration of heavy metals. However, the formation of ternary surface complexes may increase the amount of heavy metals removed from solution. As NOM is always present in natural waters, a surface partially covered by NOM is a more accurate description than a pure mineral surface. This may have implications for the adsorption of metal ions.

If the AMD is to be neutralised by liming or mixing with surface waters, different Fe(III) precipitates will form at different pH values. The ambient Zn(II) concentration at Kristineberg can by adsorption and/or precipitation be reduced to 0.3 μM at pH 5.5 and even lower amounts at higher pH. The Swedish Environmental Protection Agency classifies Zn(II) concentrations between 0.1-0.3 μM in natural waters as low with a small risk of biological effects[123], thus the results can be considered satisfactory. However, the inclusion of NOM into AMD can reduce the efficiency of natural attenuation and pH has to be increased further to achieve the same effect.

The work presented in this thesis has answered some important questions but many still remain. One concerns the acid-base properties of NOM at high pH. The adsorption of NOM to mineral surfaces is a problematic area in terms of surface complexation modelling. Filius *et al.*[124] modelled the adsorption of fulvic acids (FA) to goethite using eight pK_a values for FA between 1.67-12.47 and four different surface complexes. This type of model explains well the macroscopic effects well for extracted FA and might also provide an explanation for the adsorption of NOM as well. In the metal-schwertmannite system there are still questions to be answered before accurate models can be proposed. Two of them are: How does adsorbed SO_4^{2-} behave in the presence of metal ions? And: Do adsorbed metal ions stabilise schwertmannite and inhibiting transformation in the same way as proposed for arsenate? The formation of precipitate-like metal clusters at the schwertmannite surface is also interesting to study further. The problems and questions discussed should be resolvable given time and it is believed that the results presented and the conclusions reached provide a firm basis for continued investigations.

REFERENCES

[1] Nordstrom, D.K.; Alpers, C.N.; Ptacek, C.J.; Blowes, D.W. Negative pH and extremely acidic mine waters from Iron Mountain, California. *Environ. Sci. Technol.* 2000,*34,* 254-258.

[2] Bigham, J.M., Nordstrom, D.K. *Iron and aluminum hydroxysulfates from acid sulfate waters*. pp 351-403. In: *Reviews in mineralogy and geochemistry. Volume 40. Sulfate minerals: Crystallography, Geochemistry, and Environmental Significance*; Alpers, C.N., Jambor, J.L., Nordstrom, D.K. (Eds.). The Mineralogical Society of America, Washington DC, 2000.

[3] Carlsson. E. *Sulphide-rich tailings remediated by soil cover - Evaluation of cover efficiency and tailings geochemistry, Kristineberg, northern Sweden. Doctoral thesis*, Luleå Technical University, Luleå, 2002.

[4] Holmström, H.; Öhlander, B. Oxygen penetration and subsequent reactions in flooded sulphidic mine tailings: A study at Stekenjokk, Northern Sweden. *Appl. Geochem.* 1999,*14,* 747-759.

[5] Morales. T. *Groundwater treatment of acid mine drainage. Licentiate thesis*, Stockholm University, Stockholm, 2001.

[6] Sjöblom, Å. *Mechanisms of metal immobilisation in mine drainage treatment wetlands - A sustainability study*. pp 817-823. In: *Proceedings from the 6th International Conference on Acid Rock Drainage, Cairn, Australia. 12-18 July*; 2003.

[7] Lindsay. W.L. *Chemical equilibria in soils,* John Wiley & Sons, New York, 1979.

[8] Ebenå. G. *Sulfidic mine waste microorganisms in an ecological context. Doctoral thesis*, Linköping university, Linköping, 2003.

[9] Bhatti, T.M.; Bigham, J.M.; Carlson, L.; Tuovinen, O.H. Mineral products of pyrrhotite oxidation by Thiobacillus ferrooxidans. *Appl. Environ. Microbiol.* 1993,*59,* 1984-1990.

[10] Berger, A.C.; Bethke, C.M.; Krumhansl, J.L. A process model of natural attenuation in drainage from a historic mining district. *Appl. Geochem.* 2000,*15,* 655-666.

[11] Lee, G.; Bigham, J.M.; Faure, G. Removal of trace metals by coprecipitation with Fe, Al and Mn from natural waters contaminated with acid mine drainage in the Ducktown Mining District, Tennessee. *Appl. Geochem.* 2002,*17,* 569-581.

[12] Dinelli, E.; Tateo, F. Different types of fine-grained sediments associated with acid mine drainage in the Libiola Fe-Cu mine area (Ligurian Apennines, Italy). *Appl. Geochem.* 2002,*17,* 1081-1092.
[13] Bigham, J.M.; Schwertmann, U.; Pfab, G. Influence of pH on mineral speciation in a bioreactor simulating acid mine drainage. *Appl. Geochem.* 1996,*11,* 845-849.
[14] Bigham, J.M.; Schwertmann, U.; Traina, S.J.; Winland, R.L.; Wolf, M. Schwertmannite and the chemical modeling of iron in acid sulfate waters. *Geochim. Cosmochim. Acta* 1996,*60,* 2111-2121.
[15] Stumm. W. *Chemistry of the solid-water interface*, John Wiley & Sons, New York, 1992.
[16] Venema, P.; Hiemstra, T.; Weidler, P.G.; van Riemsdijk, W.H. Intrinsic proton affinity of reactive surface groups of metal (hydr)oxides: Application to iron (hydr)oxides. *J. Colloid Interface Sci.* 1998,*198,* 282-295.
[17] Davis, J.B., Kent, D.B. *Surface complexation modeling in aqueous geochemistry*. pp 177-260. In: *Reviews in mineralogy and geochemistry. Volume 23. Mineral-water interface geochemistry*; Hochella Jr, M.F., White, A.F. (Eds.). The Mineralogical Society of America, Washington DC, 1990.
[18] Thurman. E.M. *Organic Geochemistry of Natural Waters*, Martinus Nijhoff/Dr W Junk Publ, Dordrecht, 1985.
[19] Köhler. S. *Quantifying the role of natural organic acids on pH and buffering in Swedish surface waters, Doctoral thesis*. Swedish University of Agricultural Sciences, Umeå, 1999.
[20] Ritchie, J.D.; Perdue, E.M. Proton-binding study of standard and reference fulvic acids, humic acids, and natural organic matter. *Geochim. Cosmochim. Acta* 2003,*67,* 85-96.
[21] *Mitigation of the environmental impact from mining waste. Programme plan for the year 2003*, MiMi Print, Luleå, 2002.
[22] Atkinson, R.J.; Posner, A.M.; Quirk, J.P. Adsorption of potential-determining ions at the ferric oxide-aqueous electrolyte interface. *J. Phys. Chem.* 1967,*71,* 550-558.
[23] Brunauer, S.; Emmett, P.H.; Teller, E. Adsorption of gases in multimolecular layers. *Amer. Chem. Soc. J.* 1938,*60,* 309-319.
[24] Lövgren, L.; Sjöberg, S.; Schindler, P.W. Acid/base reactions and Al(III) complexation at the surface of goethite. *Geochim. Cosmochim. Acta* 1990,*54,* 1301-1306.

[25] Lützenkirchen, J.; Boily, J.-F.; Lövgren, L.; Sjöberg, S. Limitations of the potentiometric technique in determining the proton active site density of goethite surfaces. *Geochim. Cosmochim. Acta* 2002,*66,* 3389-3396.

[26] Ginstrup, O. Experimental and computation methods for studying multicomponent equilibria-II. An automated system for precision emf titrations. *Chem. Instrum.* 1973,*4*, 141-155.

[27] Brown, A.S. A type of silver chloride electrode suitable for use in dilute solutions. *J. Am. Chem. Soc.* 1934,*56,* 646-647.

[28] Forsling, W.; Hietanen, S.; Sillén, L.G. Studies on the hydrolysis of metal ions-III. The hydrolysis of the mercury(I) ion,Hg^{2+}_2. *Acta Chem. Scand.* 1952,*6,* 901-909.

[29] Sjöberg, S.; Hägglund, Y.; Nordin, A.; Ingri, N. Equilibrium and structural studies of silicon(IV) and aluminium(III) in aqueous solution. V. Acidity constants of silicic acid and the ionic product of water in the medium range 0.05-2.0 M Na(Cl) at 25°C. *Marine Chemistry* 1983,*13*, 35-44.

[30] Sjöberg, S.; Lövgren, L. The application of potentiometric techniques to study complexation reactions at the mineral/water interface. *Aq. Sci.* 1993,*55,* 324-335.

[31] Ingri, N.; Andersson, I.; Pettersson, L.; Yagasaki, A.; Andersson, L.; Holmström, K. LAKE- A program system for equilibrium analytical treatment of multimethod data, especially combined potentiometric and nuclear magnetic resonance data. *Acta Chem. Scand.* 1996,*50,* 717-734.

[32] Hunter. R.J. *Zeta potential in colloid science. Principle and applications*, Academic Press, London, 1988.

[33] *Powder Diffraction File*, International Centre for Diffraction Data, Newtown Square, 1997.

[34] Teo. B.K. *EXAFS: Basic principles and data analysis*, Springer-Verlag, Berlin, 1986.

[35] Jalilehvand. F. *Structure of hydrated ions and cyano complexes by X-ray absorption spectroscopy. Doctoral thesis*, Royal Institute of Technology, Stockholm, 2000.

[36] Penner-Hahn, J.E. X-ray absorption spectroscopy in coordination chemistry. *Coordination Chemistry Reviews* 1999,*190-192,* 1101-1123.

[37] Watts, J.F. *X-ray photoelectron spectroscopy*. pp 5-23. In: *Surface science techniques*; Walls, J.M., Smith, R. (Eds.). Pergamon, Oxford, 1994.

[38] Moulder, J.F., Stickle, W.F., Sobol, P.E., Bomben, K.D. In: *Handbook of x-ray photoelectron spectroscopy*; Chastain, J., King Jr, R.C. (Eds.). Physical Electronics, Inc., Eden Prairie, 1995.

[39] Vincent. A. *Molecular symmetry and group theory*, John Wiley & Sons, Chichester, 1977.

[40] Nakamoto. K. *Infrared and Raman spectra of inorganic and coordination compounds Part B: Applications in coordination, organometallic, and bioinorganic chemistry. 5th edition*, John Wiley & Sons, Inc., New York, 1997.

[41] Axe, K.; Persson, P. Time-dependent surface speciation of oxalate at the water-boehmite (γ-AlOOH) interface: Implications for dissolution. *Geochim. Cosmochim. Acta* 2001,*65*, 4481-4492.

[42] Glocker, E.F. Über einen neuen Eisensinter von Obergrund bie Zuckmantel. *Poggendorff's Annalen Physik Chemie* 1853,*89*, 482-488.

[43] Fojt, B. On the problem of glockerite as a secondary mineral of ore deposits. *Scripta Fac Sci Nat UJEP Brunensis, Geologia I* 1975,*5*, 5-20.

[44] Cornell. R.M., Schwertmann. U. *The iron oxides: Structure, properties, reactions, occurrence and uses*, VCH Verlagsgesellschaft mbH, Weinheim, 1996.

[45] Bigham, J.M.; Schwertmann, U.; Carlson, L.; Murad, E. A poorly crystallized oxyhydroxysulfate of iron formed by bacterial oxidation of Fe(II) in acid mine waters. *Geochim. Cosmochim. Acta* 1990,*54*, 2743-2758.

[46] Bigham, J.M.; Carlson, L.; Murad, E. Schwertmannite, a new iron oxyhydroxysulphate from Pyhäsalmi, Finland, and other localities. *Mineral. Mag.* 1994,*58*, 641-648.

[47] Schwertmann, U.; Fojt, B. Schwertmannite - ein neues mineral und seine geschichte. *Lapis* 1996,33-34.

[48] Schwertmann, U.; Bigham, J.M.; Murad, E. The first occurrence of schwertmannite in a natural stream environment. *Eur. J. Mineral.* 1995,*7*, 547-552.

[49] Fitzpatrick, R.W.; Self, P.G. Iron oxyhydroxides, sulfides and oxyhydroxysulfates as indicators of acid sulfate weathering environments. *Advances in GeoEcology* 1997,*30*, 227-240.

[50] Kawano, M.; Tomita, K. Geochemical modeling of bacterially induced mineralization of schwertmannite and jarosite in sulfuric acid spring water. *Am. Mineral.* 2001,*86*, 1156-1165.

[51] Bishop, J.L.; Pieters, C.M.; Burns, R.G.; Edwards, J.O.; Mancinelli, R.L.; Fröschl, H. Reflectance spectroscopy of ferric sulfate-bearing montmorillonites as Mars soil analog materials. *Icarus* 1995,*117,* 101-119.

[52] Morris, R.V.; Golden, D.C. Goldenrod pigments and the occurrence of hematite and possibly goethite in the Olympus-Amazonis region of Mars. *Icarus* 1998,*134,* 1-10.

[53] Claassen, J.O.; Meyer, E.H.O.; Rennie, J.; Sandenbergh, R.F. Iron precipitation from zinc-rich solutions: defining the Zincor Process. *Hydrometallurgy* 2002,*67,* 87-108.

[54] Yu, J.-Y.; Heo, B.; Cho, J.-P.; Chang, H.-W. Apparent solubilities of schwertmannite and ferrihydrite in natural stream waters polluted by mine drainage. *Geochim. Cosmochim. Acta* 1999,*63,* 3407-3416.

[55] Kim, J.J.; Kim, S.J. Environmental, mineralogical, and genetic characterization of ochreous and white precipitates from acid mine drainage in Taebaeg, Korea. *Environ. Sci. Technol.* 2003,*37,* 2121-2126.

[56] Kim, J.J.; Kim, S.J.; Tazaki, K. Mineralogical characterization of microbial ferrihydrite and schwertmannite, and non-biogenic Al-sulfate precipitates from acid mine drainage in the Donghae mine area, Korea. *Environ. Geol.* 2002,*42,* 19-31.

[57] Briggs, D., Seah, M.P. (Eds.) *Practical surface analysis. Volume 1. Auger and x-ray photoelectron spectroscopy*; John Wiley & Sons, Chichester, 1990.

[58] Yu, J.-Y.; Park, M.; Kim, J. Solubilities of synthetic schwertmannite and ferrihydrite. *Geochem. J.* 2002,*36,* 119-132.

[59] Boily, J.-F.; Lützenkirchen, J.; Balmès, O.; Beattie, J.; Sjöberg, S. Modeling proton binding at the goethite (α-FeOOH)-water interface. *Colloid Surf. A-Physicochem. Eng. Asp.* 2001,*179,* 11-27.

[60] Zänker, H.; Moll, H.; Richter, W.; Brendler, V.; Henning, C.; Reich, T.; Kluge, A.; Hüttig, G. The colloid chemistry of acid rock drainage solution from an abandoned Zn-Pb-Ag mine. *Appl. Geochem.* 2002,*17,* 633-648.

[61] Dold. B. *Mineralogical and geochemical changes of copper flotation tailings in relation to their original composition and climatic setting - Implications for acid mine drainage and element mobility, Doctoral thesis* Univesité de Genève, Geneva, 1999.

[62] Schwertmann, U. Differenzierung der eisenoxide des bodens durch extration mit ammoniumoxalat-lösung. *Z. Pflanzenernahr. Bodenknd.* 1964,*105,* 194-202.

[63] Dold, B. Dissolution kinetics of schwertmannite and ferrihydrite in oxidized mine samples and their detection by differential X-ray diffraction (DXRD). *Appl. Geochem.* 2003,*18*, 1531-1540.
[64] Barham, B.J. Schwertmannite: A unique mineral, contains a replaceable ligand, transforms to jarosites, hematites, and/or basic iron sulfate. *J. Mater. Res.* 1997,*12*, 2751-2757.
[65] Chon, H.-T.; Kim, J.-Y.; Choi, S.-Y. Hydrogeochemical characterisation of acid mine drainage around the abandoned Youngdong coal mine in Korea. *Resour. Geol* 1999,*49*, 113-120.
[66] Peak, D.; Ford, R.G.; Sparks, D.L. An *in situ* ATR-FTIR investigation of sulfate bonding mechanisms on goethite. *J. Colloid Interface Sci.* 1999,*218*, 289-299.
[67] Kim, J.-Y.; Chon, H.-T. Pollution of a water course impacted by acid mine drainage in the Imgok creek of the Gangreung coal field, Korea. *Appl. Geochem.* 2001,*16*, 1387-1396.
[68] Mazzetti, L.; Thistlethwaite, P.J. Raman spectra and thermal transformation of ferrihydrite and schwertmannite. *J. Raman Spectrosc.* 2002,*33*, 104-111.
[69] Peine, A.; Tritschler, A.; Küsel, K.; Peiffer, S. Electron flow in an iron-rich acidic sediment - evidence for an acidity-driven iron cycle. *Limnology and Oceanography* 2000,*45*, 1077-1087.
[70] Karathanasis, A.D.; Thompson, Y.L. Mineralogy of iron precipitates in a constructed acid mine drainage wetland. *Soil Sci. Soc. Am. J.* 1995,*59*, 1773-1781.
[71] Childs, C.W.; Inoue, K.; Mizota, C. Natural and anthropogenic schwertmannites from Towada-Hachimantai National Park, Honshu, Japan. *Chem. Geol.* 1998,*144*, 81-86.
[72] Scheinost, A.C.; Schwertmann, U. Color identification of iron oxides and hydroxysulfates: Use and limitation. *Soil Sci. Soc. Am. J.* 1999,*63*, 1463-1471.
[73] Williams, D.J.; Bigham, J.M.; Cravotta III, C.A.; Traina, S.J.; Anderson, J.E.; Lyon, J.G. Assessing mine drainage pH from the color and spectral reflectance of chemical precipitates. *Appl. Geochem.* 2002,*17*, 1273-1286.
[74] Regenspurg, S.; Gößner, A.; Pfeiffer, S.; Küsel, K. Potential remobilization of toxic anions during reduction of arsenated and chromated schwertmannite by the dissimilatory Fe(III)-reducing bacterium *Acidiphilium cryptum* JF-5. *Water Air Soil Pollut. Focus* 2002,*2*, 57-67.

[75] Yu, J.-Y.; Heo, B.; Chang, H.-W. Stability of schwertmannite and ferrihydrite in the stream waters of Imgok and Osheep Creek polluted by acid mine drainage. *Mineral. Mag.* 1998,*62A*, 1675-1676.

[76] Anderson, M.A.; Tejedor-Tejedor, M.I.; Stanforth, R.R. Influence of aggregation on the uptake kinetics of phosphate by goethite. *Environ. Sci. Technol.* 1985,*19*, 632-637.

[77] Persson, P.; Lövgren, L. Potentiometric and spectroscopic studies of sulfate complexation at the goethite-water interface. *Geochim. Cosmochim. Acta* 1996,*60*, 2789-2799.

[78] Rose, S.; Ghazi, M. Release of sorbed sulfate from iron oxyhydroxides precipitated from acid mine drainage associated with coal mining. *Environ. Sci. Technol.* 1997,*31*, 2136-2140.

[79] Rose, S.; Elliott, W.C. The effect of pH regulation upon the release of sulfate from ferric precipitates formed in acid mine drainage. *Appl. Geochem.* 2000,*15*, 27-34.

[80] Lintnerová, O.; Šefcíková, B. Sorption and desorption of metals and sulfates by iron oxyhydroxides in sulfide mine waste. *Mineral. Slovaca* 2002,*34*, 219-232.

[81] Hug, S.J. *In situ* Fourier Transform Infrared measurement of sulfate adsorption on hematite in aqueous solutions. *J. Colloid Interface Sci.* 1997,*188*, 415-422.

[82] Tipping. E. *Cation binding by humic substances*, Cambridge university press, Cambridge, 2002.

[83] Köhler, S.; Laudon, H.; Wilander, A.; Bishop, K. Estimating organic acid dissociation in natural surface waters using total alkalinity and TOC. *Wat. Res.* 2000,*106*, 55-65.

[84] Swift, R.S. *Organic matter characterization*. pp 1011-1069. In: *Methods of soil analysis, Part 3: Chemical methods*; Sparks, D.L. (Ed.). American Society of Agronomy, 1996.

[85] Stumm. W., Morgan. J.J. *Aquatic chemistry. 2nd edition*, John Wiley & sons, New York, 1981.

[86] Lövgren, L.; Hedlund, T.; Öhman, L.-O.; Sjöberg, S. Equilibrium approaches to natural water systems-6. Acid-base properties of a concentrated bog-water and its complexation reactions with aluminium(III). *Wat. Res.* 1987,*21*, 1401-1407.

[87] Tipping, E.; Hurley, M.A. A unifying model of cation binding by humic substances. *Geochim. Cosmochim. Acta* 1992,*56*, 3627-3641.

[88] Köhler, S.J.; Hruška, J.; Bishop, K. Influence of organic acid site density on pH modelling of Swedish lakes. *Can. J. Fish. Aq. Sci.* 1999,*56,* 1461-1470.

[89] Lindgren, J.; Öhman, L.-O. Characterization of acid/base properties for bleached softwood fibres as influenced by ionic medium. *Nordic Pulp Paper Res. J.* 2000,*15,* 18-23.

[90] Bergelin. A. *Acid-base properties and aggregation of humic materials. Doctoral thesis,* Royal Institute of Technology, Stockholm, 2001.

[91] Webster, J.G.; Swedlund, P.J.; Webster, K.S. Trace metal adsorption onto an acid mine drainage iron(III) oxy hydroxy sulfate. *Environ. Sci. Technol.* 1998,*32,* 1361-1368.

[92] Swedlund, P.J.; Webster, J.G. Cu and Zn ternary surface complex formation with SO_4 on ferrihydrite and schwertmannite. *Appl. Geochem.* 2001,*16,* 503-511.

[93] Randall, S.R.; Sherman, D.M.; Ragnarsdottir, K.V. An EXAFS investigation of the mechanism of Cd attenuation on Fe and Mn (oxyhydr)oxide minerals. *Mineral. Mag.* 1998,*62A,* 1231-1232.

[94] Randall, S.R.; Sherman, D.M.; Ragnarsdottir, K.V.; Collins, C.R. The mechanism of cadmium surface complexation on iron oxyhydroxide minerals. *Geochim. Cosmochim. Acta* 1999,*63,* 2971-2987.

[95] Walter, M.; Arnold, T.; Reich, T.; Bernhard, G. Sorption of uranium(VI) onto ferric oxides in sulfate-rich acid waters. *Environ. Sci. Technol.* 2003,*37,* 2898-2904.

[96] Carlson, L.; Bigham, J.M.; Schwertmann, U.; Kyek, A.; Wagner, F. Scavenging of As from acid mine drainage by schwertmannite and ferrihydrite: A comparison with synthetic analogues. *Environ. Sci. Technol.* 2002,*36,* 1712-1719.

[97] Waychunas, G.A.; Xu, N.; Fuller, C.C.; Davis, J.A.; Bigham, J.M. XAS study of AsO_{43-} and SeO_{42-} substituted schwertmannites. *Physica B* 1995,*208&209,* 481-483.

[98] Fukushi, K.; Sato, T.; Yanase, N. Sorption of As(V) on schwertmannite and its effect on the transformation. *Geochim. Cosmochim. Acta* 2002,*66/SI,* A249

[99] Fukushi, K.; Sasaki, M.; Sato, T.; Yanase, N.; Amano, H.; Ikeda, H. A natural attenuation of arsenic drainage from an abandoned arsenic mine dump. *Appl. Geochem.* 2003,*18,* 1267-1278.

[100] Palmqvist, U.; Ahlberg, E.; Lövgren, L.; Sjöberg, S. *In situ* voltammetric determinations of metal ions in goethite suspensions: Single metal ion systems. *J. Colloid Interface Sci.* 1997,*196,* 254-266.

[101] Persson, I.; Persson, P.; Sandström, M.; Ullström, A.-S. Structure of Jahn-Teller distorted solvated copper(II) ions in solution, and in solids with apparently regular octahedral coordination geometry. *J. Chem. Soc. [Dalton Trans.]* 2002,*7,* 1256-1266.

[102] Bochatay, L.; Persson, P.; Lövgren, L.; Brown Jr, G.E. XAFS study of Cu(II) at the water-goethite (α-FeOOH) interface. *Journal de Physique IV France* 1997,*7,* 819-820.

[103] Parkman, R.H.; Charnock, J.M.; Bryan, N.D.; Livens, F.R.; Vaughan, D.J. Reaction of copper and cadmium ions in aqueous solution with goethite, lepidocrocite, mackinawite, and pyrite. *Am. Mineral.* 1999,*84,* 407-419.

[104] Parida, K.M.; Goria, B.; Das, N.N.; Rao, S.B. Studies on ferric oxide hydroxides. III. Adsorption of selenite (SeO_{32-}) on different forms of iron oxyhydroxides. *J. Colloid Interface Sci.* 1997,*185,* 355-362.

[105] Kanungo, S.B. Adsorption of cations on hydrous oxides of iron I. Interfacial behavior of amorphous FeOOH and β-FeOOH (akaganeite) in different electrolyte solutions. *J. Colloid Interface Sci.* 1994,*162,* 86-92.

[106] Dzombak. D.A., Morel. F.M.M. *Surface Complexation Modeling. Hydrous Ferric Oxide*, John Wiley & Sons, New York, 1990.

[107] Davis, J. Adsorption of natural dissolved organic matter at the oxide/water interface. *Geochim. Cosmochim. Acta* 1982,*46,* 2381-2393.

[108] Spark, K.M.; Wells, J.D.; Johnson, B.B. Characteristics of the sorption of humic acid by soil minerals. *Aust. J. Soil Res.* 1997,*35,* 103-112.

[109] Tipping, E.; Cooke, D. The effects of adsorbed humic substances on the surface charge of goethite (α-FeOOH) in fresh water. *Geochim. Cosmochim. Acta* 1982,*46,* 75-80.

[110] Parfitt, R.L.; Fraser, A.R.; Farmer, A.C. Adsorption on hydrous oxides. III. Fulvic acid and humic acid on goethite, gibbsite and imogolite. *J. Soil Sci.* 1977,*28,* 289-296.

[111] Gu, B.; Schmitt, J.; Chen, Z.; Liang, L.; McCarthy, J. Adsorption and desorption of natural organic matter on iron oxide: mechanisms and models. *Environ. Sci. Technol.* 1994,*28,* 38-46.

[112] Avena, M.J.; Koopal, L.K. Desorption of humic acids from an iron oxide surface. *Environ. Sci. Technol.* 1998,*32,* 2572-2577.
[113] Vermeer, A.W.P.; van Riemsdijk, W.H.; Koopal, L.K. Adsorption of humic acid to mineral particles. 1. Specific and electrostatic interactions. *Langmuir* 1998,*14,* 2810-2819.
[114] Day, G.; Hart, B.; McKelvie, I.; Beckett, R. Adsorption of natural organic matter onto goethite. *Colloid Surf. A-Physicochem. Eng. Asp.* 1994,*89,* 1-13.
[115] Gu, B.; Schmitt, J.; Chen, Z.; Liang, L.; McCarthy, J. Adsorption and desorption of different organic matter fractions on iron oxide. *Geochim. Cosmochim. Acta* 1995,*59,* 219-229.
[116] Tipping, E.; Griffith, J.R.; Hilton, J. The effect of adsorbed humic substances on the uptake of copper(II) by goethite. *Croat. Chem. Acta* 1983,*56,* 613-621.
[117] Nowack, B. Environmental chemistry of aminopolycarboxylate chelating agents. *Environ. Sci. Technol.* 2002,*36,* 4009-4016.
[118] Sheals, J.; Granström, M.; Sjöberg, S.; Persson, P. Coadsorption of Cu(II) and glyphosate at the water-goethite (α-FeOOH) interface: molecular structures from FTIR and EXAFS measurements. *J. Colloid Interface Sci.* 2003,*262,* 38-47.
[119] Alcacio, T.E.; Hesterberg, D.; Chou, J.W.; Martin, J.D.; Beauchemin, S.; Sayers, D.E. Molecular scale characteristics of Cu(II) bonding in goethite-humate complexes. *Geochim. Cosmochim. Acta* 2001,*65,* 1355-1366.
[120] Vermeer, A.W.P.; McCulloch, J.K.; van Riemsdijk, W.H.; Koopal, L.K. Metal ion adsorption to complexes of humic acid and metal oxides: Deviations from the additivity rule. *Environ. Sci. Technol.* 1999,*33,* 3892-3897.
[121] Lövgren, L.; Sjöberg, S. Equilibrium approaches to natural water systems - 7. Complexation reactions of copper(II), cadmium(II) and mercury(II) with dissolved organic matter in a concentrated bog-water. *Wat. Res.* 1989,*23,* 327-332.
[122] Milne, C.J.; Kinniburgh, D.G.; van Riemsdijk, W.H.; Tipping, E. Generic NICA-Donnan model parameters for metal-ion binding by humic substances. *Environ. Sci. Technol.* 2003,*37,* 958-971.
[123] *Environmental Quality Criteria for Lakes and Watercourses (In Swedish)*, Naturvårdsverket, Swedish EPA, Stockholm, 1999.
[124] Filius, J.D.; Lumsdon, D.G.; Meeussen, C.L.; Hiemstra, T.; van Riemsdijk, W.H. Adsorption of fulvic acid on goethite. *Geochim. Cosmochim. Acta* 2000,*64,* 51-60.

ACKNOWLEDGMENTS

There are a lot of people that I would like to thank. First of all, Docent Lars Lövgren who took me on as a PhD-student even if I was “a bit on the old side”. Thank you for all support, help, ideas and travelling over the years. Also a big thank you to my other supervisors, Docent Per Persson and Prof. Staffan Sjöberg for everything from discussing chemistry to mushroom soup and having a good time.

MiMi and MISTRA are gratefully acknowledged for giving me money to spend during the last five years. I’ve learnt a lot from the PhD students in MiMi, e.g. how to get lost with a canoe going down-stream (Åsa and Eva), how to drive off-road in Kristineberg (Teresita), how to get as many standard deviations as possible on one slide (Erik) and that the best way of losing your hotel key is to throw it into a pond (Sally). From the rest of the people in MiMi I’ve picked up some useful things even if you aren’t all PhD-students.

To all you people, past and present, at Inorganic chemistry, who make the department such a good place to work. A special thank you to Agneta and Ingegärd for all the little and big things you have done, Andrei for XPS measurements and “Russian parties”, Dan and Ann for help with the XRD measurements and Lars-Olof for making me interested in the field of inorganic chemistry over a decade ago.

Thank you all you PhD-students for all the things we have done together over the years. A special thank you to Fabian for making me smile at the lunch breaks and laugh at the squash court and to my travelling companions Madeleine and Åsa.

A big thank you to my room mates. Johan, for giving me both lodging and a map to LAKE-country. Katarina, your poker face will never be forgotten.

Thank you to my Swedish family, especially Bengt and Eva. This would not have been written without your hard work.

Thank you to my new English family for making me feel very welcome. We’ll see much more of each other soon…

To my truly old friends from the medieval society, a big thank you for all the things we have done and experienced over the years.

To all the rest of my friends who doesn’t fit into any of the above mentioned categories, you are not forgotten!

Finally Julia, my wife, soul mate, colleague and “särbo”. It’s slightly worrying when your wife moves back to her parents a month after the wedding but now we will finally be reunited. Thank you for everything! xxx